Evaluation of global simulations of aerosol particle number and cloud condensation nuclei, and implications for cloud droplet formation

George S. Fanourgakis[1], Maria Kanakidou[1], Athanasios Nenes[2,3,4,5], Susanne E. Bauer[6,7], Tommi Bergman[8], Ken S. Carslaw[9], Alf Grini[10], Douglas S. Hamilton [11], Jill S. Johnson[9], Vlassis A. Karydis[12,13], Alf Kirkevåg[14], John K. Kodros[15], Ulrike Lohmann[16], Gan Luo[17], Risto Makkonen[18,19], Hitoshi Matsui[20], David Neubauer[16], Jeffrey R. Pierce [15], Julia Schmale [21], Philip Stier[22], Kostas Tsigaridis [7,6], Twan van Noije[8], Hailong Wang[23], Duncan Watson-Parris[22], Daniel M. Westervelt[24,6], Yang Yang[23], Masaru Yoshioka[9], Nikos Daskalakis[25], Stefano Decesari[26], Martin Gysel Beer[21], Nikos Kalivitis[1], Xiaohong Liu[27], Natalie M. Mahowald[11], Stelios Myriokefalitakis[28], Roland Schrödner[29], Maria Sfakianaki[1], Alexandra P. Tsimpidi[12], Mingxuan Wu[27], Fangqun Yu[17]

[1]Environmental Chemical Processes Laboratory, Department of Chemistry, University of Crete, Heraklion, 70013, Greece

[2]Laboratory of Atmospheric Processes and their Impacts, School of Architecture, Civil & Environmental Engineering, Ecole Polytechnique Federale de Lausanne, Lausanne, 1015, Switzerland

[3]IERSD, National Observatory of Athens, P. Penteli 15236, Athens, Greece

[4] ICE-HT, Foundation for Research and Technology – Hellas, Greece

[5]School of Earth and Atmospheric Sciences, Georgia Institute of Technology, Atlanta, GA, 30332-0340, USA

[6] NASA Goddard Institute for Space Studies, New York NY USA

[7] Center for Climate Systems Research, Columbia University, New York NY USA

[8] Royal Netherlands Meteorological Institute (KNMI), DeBilt, Netherlands

[9] School of Earth and Environment, University of Leeds, UK

[10] independent researcher

[11] Department of Earth and Atmospheric Sciences, Atkinson Center for a Sustainable Future, Cornell University, Ithaca, NY, USA.

[12] Department of Atmospheric Chemistry, Max Planck Institute for Chemistry, Mainz, German

[13]Forschungszentrum Jülich, Inst Energy & Climate Res IEK-8, D-52425 Jülich, Germany

[14] Norwegian Meteorological Institute, Oslo, Norway

[15] Department of Atmospheric Science, Colorado State University, Fort Collins, Colorado, USA

[16] ETH Zurich, Institute for Atmospheric and Climate Science, Zurich, Switzerland

[17] The Atmospheric Sciences Research Center (ASRC), of the State University of New York at Albany

[18] System Research, Finnish Meteorological Institute, P.O. Box 503, 00101, Helsinki, Finland

[19] Institute for Atmospheric and Earth System Research / Physics, University of Helsinki, P.O. Box 64, 00014 Helsinki, Finland

[20] Graduate School of Environmental Studies, Nagoya University, Nagoya, Japan.

[21] Laboratory of Atmospheric Chemistry, Paul Scherrer Institute, Villigen, Switzerland

[22] Atmospheric, Oceanic & Planetary Physics, Department of Physics, University of Oxford, UK

[23] Atmospheric Sciences and Global Change Division, Pacific Northwest National Laboratory, Richland, Washington, USA

[24] Lamont-Doherty Earth Observatory, Columbia University, Palisades, NY, USA, 10964

[25] Laboratory for Modeling and Observation of the Earth System (LAMOS) Institute of Environmental Physics (IUP), University of Bremen, Bremen, Germany

[26] Institute of Atmospheric Sciences and Climate, National Research Council of Italy, Via Piero Gobetti, 101, 40129 Bolonga, Italy

[27] Department of Atmospheric Science, University of Wyoming, Laramie, Wyoming, USA

[28] Institute for Environmental Research and Sustainable Development, National Observatory of Athens, Penteli, Greece

[29] Centre for Environmental and Climate Research, Lund University, Sweden

Correspondence to: Maria Kanakidou (mariak@uoc.gr), Athanasios Nenes (athanasios.nenes@epfl.ch)

Abstract. A total of sixteen global chemistry transport models and general circulation models have participated in this study. Fourteen models have been evaluated with regard to their ability to reproduce near-surface observed number concentration of aerosol particle and cloud condensation nuclei (CCN), and derived cloud droplet number concentration (CDNC). Model results for the period 2011-2015 are compared with aerosol measurements (aerosol particle number, CCN and aerosol particle composition in the submicron fraction) from nine surface stations, located in Europe and Japan. The evaluation focuses on the ability of models to simulate the average across time state in diverse environments, and on the seasonal and short-term variability in the aerosol properties.

There is no single model that systematically performs best across all environments represented by the observations. Models tend to underestimate the observed aerosol particle and CCN number concentrations, with average normalized mean bias (NMB) of all models and for all stations, where data are available, of -24% and -35% for particles with dry diameters > 50nm and >120 nm and -36% and -34% for CCN at supersaturations of 0.2% and 1.0%, respectively. Fifteen models have been used to produce ensemble annual median distributions of relevant parameters. The model diversity (defined as the ratio of standard deviation to mean) is up to about 3 for simulated N_3 (number concentration of particles with dry diameters larger than 3 nm) and up to about 1 for simulated CCN in the extra-polar regions.

An additional model has been used to investigate potential causes of model diversity in CCN and bias compared to the observations by performing a perturbed parameter ensemble (PPE) accounting for uncertainties in 26 aerosol-related model input parameters. This PPE suggests that biogenic secondary organic aerosol formation and the hygroscopic properties of the

organic material are likely to be the major sources of CCN uncertainty in summer, with dry deposition and cloud processing being dominant in winter.

Models capture the relative amplitude of seasonal variability of the aerosol particle number concentration for all studied particle sizes with available observations (dry diameters larger than 50, 80 and 120 nm). The short-term persistence time (on

5 the order of a few days) of CCN concentrations, which is a measure of aerosol dynamic behavior in the models, is underestimated on average by the models by 40% during winter and 20% in summer.

In contrast to the large spread in simulated aerosol particle and CCN number concentrations, the CDNC derived from simulated CCN spectra is less diverse and in better agreement with CDNC estimates consistently derived from the observations (average NMB -17% and -22% for updraft velocities 0.3 and 0.6 m.s^{-1}, respectively). In addition, simulated

10 CDNC is in slightly better agreement with observationally-derived value at lower than at higher updraft velocities (index-of-agreement of 0.47 vs 0.50). The reduced spread of CDNC compared to that of CCN is attributed to the sublinear response of CDNC to aerosol particle number variations and the negative correlation between the sensitivities of CDNC to aerosol particle number concentration and to updraft velocity. Overall, we find that while CCN is controlled by both aerosol particle number and composition, CDNC is sensitive to CCN at low and moderate CCN concentrations and to the updraft velocity

15 when CCN levels are high.

1 Introduction

Aerosol particles absorb and scatter radiation, thereby modulating the planetary radiative balance (Boucher et al., 2013; Myhre et al., 2013). They also provide the nuclei upon which cloud droplets and ice crystals form; variations thereof can profoundly impact cloud formation and precipitation. Both the direct radiative effects of aerosols and their impacts on clouds

20 are thought to be important for climate at global and regional scales, although they are highly uncertain and confound projections of anthropogenic climate change (e.g., Boucher et al., 2013; Seinfeld et al., 2016). The impacts of aerosols on clouds in particular introduce considerable uncertainty in our estimates of equilibrium climate sensitivity and transient climate response to the combined changes in aerosol and greenhouse gases concentrations (e.g., Seinfeld et al., 2016; Fan et al. 2016).

25 Aerosols can be either directly emitted from a variety of sources (primary aerosols) or formed by nucleation from precursor compounds (secondary aerosols), which afterwards can grow by condensation and coagulation from a few nanometers to a few hundreds of nanometers (Kerminen et al., 2012). Note that secondary aerosol also includes the condensed material upon primary emitted aerosol. Aerosols that have the potential to create cloud droplets at atmospherically-relevant conditions are termed cloud condensation nuclei (CCN). The CCN number concentration depends

30 on the particle size distribution, chemical composition and mixing state, as well as the level of water vapor supersaturation that develops in rising air parcels (Köhler, 1936; Seinfeld and Pandis, 2006). It is now established that primary emissions of particulate matter and particle formation from anthropogenic precursor gases have strongly modulated clouds and climate at

the global scale since the industrial revolution (Boucher et al., 2013). Much work remains, however, to reduce the uncertainty associated with anthropogenic aerosol-cloud-climate interactions.

Among the main sources of uncertainty in simulating aerosol microphysics at regional to global scales are the amounts of particle and precursor vapor mass emitted by anthropogenic activities or natural sources, as well as the size distribution of

5   the emitted particles and their representation in models. However, Mann et al. (2012) showed that a careful choice of the aerosol parameters describing the aerosol distribution can reduce differences between the sectional and the modal description of aerosol microphysics in most parts of the atmosphere. Furthermore, carbonaceous combustion aerosol, although assumed hydrophobic upon emission was found to contribute up to 64% of global surface CCN concentrations (Spracklen et al., 2011). Although less important than particle size, particle chemical composition determines aerosol hygroscopicity

10   (Twomey, 1977; Dusek et al., 2006; Petters and Kreidenweis, 2007; Cubison et al., 2008; Bougiatioti et al., 2017). Adequate description of aerosol hygroscopicity is required to accurately describe CCN and cloud droplet number variability. In this respect, uncertainties are partially related to the organic fraction of aerosols (OA), which can be composed of thousands compounds with different physical and chemical properties. OA contributes to the fine aerosol mass by up to 30-70% depending on location and season (Kanakidou et al., 2005; Jimenez et al., 2009); while source estimates of OA are spanning

15   one order of magnitude (see the AeroCom phase-II intercomparison study of 31 models by Tsigaridis et al. (2014)). Regionally, sea salt (SS) and mineral dust (DU) are also significant contributors to the total aerosol particle mass and number concentration. Atmospheric mass loads during the first phase of AeroCom showed a high diversity among 15 models of 54% for SS and 40% for DU (Textor et al., 2006). This diversity arises from the different parameterizations used to calculate the size-resolved fluxes and their dependence on wind speed but also from the consideration, or not, of the super coarse aerosol

20   fraction (Huneeus et al., 2011; Tsigaridis et al., 2013). Although nitrate (NO_3^-) and ammonium (NH_4^+) are not explicitly studied here, differences up to a factor of 13 in the atmospheric burden of NO_3^- and 17 and 4 for NH_3 and NH_4^+, respectively, have been found between AEROCOM models (Bian et al., 2017).

Formation of new particles by nucleation in the atmosphere is a frequent phenomenon in the free troposphere and in the continental boundary layer (e.g. Kerminen et al., 2010; Kulmala and Kerminen, 2008) and an important source of aerosol

25   particle number on a global scale (Kerminen et al., 2012; Kalivitis et al., 2015; Gordon et al., 2017). Although it is well established that sulfuric acid, due to its low volatility, plays a central role in new particle formation and growth, it cannot explain the observed substantial growth of small particles in many environments where organics and NH_3 are abundant. This is due to the low concentration of sulfuric acid and is evidenced by the observed poor correlation of its concentration with the very small particles (e.g. Pierce et al., 2011). Recently, the involvement of organics from early stages of nucleation and

30   growth of particles has been established (e.g. D'Andrea et al., 2013; Spracklen et al., 2008; Makkonen et al., 2009; Tröstl et al., 2016). Several approaches for modeling particle growth in large-scale models have been developed, which are very sensitive to the volatility of organic vapors (e.g. Laaksonen et al., 2008; Yu, 2011; D'Andrea et al., 2013) and are being implemented in global models.

The number concentration and the size of cloud droplets depend both on the concentrations of CCN and on the cloud updraft velocity (Pruppacher and Klett, 1997; Seinfeld and Pandis, 2016). However, the spatial scale of updrafts governing droplet formation is several orders of magnitude smaller than the size of the grid boxes of global models. Therefore, parameterized aerosol-cloud interactions in climate models require sub-grid scale vertical velocity distributions to calculate

5   grid-scale relevant cloud droplet number concentration (CDNC) (Morales et al., 2010). Karydis et al. (2012) and Moore et al. (2013) have shown that in regions with low particle number concentrations, such as the Arctic and remote oceans, CDNC is more sensitive to CCN uncertainty than in continental regions where particle number concentrations exceed 10^4 cm^{-3}. In contrast, Ervens et al. (2010) pointed out that at high updraft velocities, supersaturation is controlled by adiabatic cooling, and CDNC is not very sensitive to errors in simulated CCN number concentration. They estimated that uncertainties in the

10   chemical composition of aerosol particles that could lead to a doubling of CCN concentration, would affect CDNC by only about 10-20%. Therefore, there are two distinct regimes with regard to CDNC sensitivity: the aerosol-limited and the updraft velocity-limited ones (Reutter et al., 2009).

    Totally opposite cloud radiative (indirect) effects could be computed by climate models depending on the dominance of CDNC sensitivity to either aerosol or updraft velocity (Sullivan et al., 2016). Therefore, capturing the balance between the

15   two is critical in understanding where and when aerosol emissions are governing the variability of cloud properties and where the updraft velocity is the controlling factor. Failure of state-of-the-art models to capture such sensitivity implies that even if models exhibit similar magnitude of aerosol indirect effects, it may be for completely different reasons (Sullivan et al., 2016). In this case models would show limited skills and their predictions would be associated with low confidence.

    The aims of this work are to *i*) assess the accuracy of state-of-the-art global aerosol models in simulating the chemical

20   composition and number concentration of aerosol particles, with focus on CCN concentrations at various water vapor supersaturation ratios, *ii*) document the diversity of the global models in simulating these aerosol properties, *iii*) produce an ensemble view of the global distribution of aerosol particle and CCN number concentrations, together with the most important particle chemical components at the Earth's surface, *iv*) evaluate the agreement of inferred CDNC from modeled and from observed CCN spectra and their sensitivity to aerosol number concentrations and updraft velocities, *v*) evaluate the

25   potential causes of model diversity and bias versus observations using model uncertainty analysis, and, *vi*) provide recommendations for future model improvements.

    Sixteen global models contributed to this study, and multi-year observations of CCN, size-resolved particle number concentration distributions, and particle chemical composition obtained from eight atmospheric monitoring stations in Europe and one in Japan were used as observational reference, representing distinct atmospheric environments (Schmale et

30   al., 2017, 2018).

2 Methodology

2.1 Contributing models and model description

Model set-up, such as spatial resolution, meteorological conditions and emission inventories differ significantly among models (supplementary Tables S1 to S3). The spatial resolution varies among the models from 0.94° by 1.3° to 4° by 5.0°

5   (latitude by longitude) and from 25 to 56 vertical layers up to 10 and even 0.1 hPa. Nine of the models are general circulation models (GCMs) and six are chemical transport models (CTMs). The CTMs use prescribed (and different) meteorological data sets; while the GCMs (with the exception of GISS-E2-TOMAS) are nudged to various reanalysis products. Atmospheric transport, secondary aerosol formation and removal of aerosols are driven by wind, temperature, radiation, precipitation and relative humidity, as well as cloud fraction and liquid water content. In addition, most of the

10   models use wind-driven dust, sea salt, and marine organic aerosol emissions as well as online biogenic emissions of non-methane volatile organic compounds (NMVOC) (Table S3). Therefore, meteorology significantly affects number concentration, composition and other metrics of aerosol particles.

Despite the recognized importance of organic compounds in nucleation (Tröstl et al., 2016), several global models that participated in the present study use one of the different binary homogeneous nucleation of sulfuric acid and water (referred

15   later as BHN e.g. Kulmala et al. (1998), Vehkamäki (2002)) and contribution of organics to particle growth (see supplementary section S1 and Table S2 and references therein). GEOS-chem-TOMAS assumes ternary nucleation mechanism when NH_3 is present and a binary one when NH_3 is absent. GEOS-Chem-APM and CAM5-Chem-APM employ ternary ion-mediated nucleation (TIMN) scheme which considers both binary and ternary as well as ion-mediated and neutral nucleation (Yu et al., 2018). New particle formation in TM5 is calculated as combination of BHN and organic-

20   sulfuric acid nucleation (Riccobono et al., 2014).

Once in the atmosphere, aerosols undergo transformations through chemical and physical processes, such as coagulation, condensation and evaporation that modify their size and physical and chemical properties. These aerosol microphysical processes are parameterized differently in models. Eight of the models use modal schemes in which the evolution of particle number and mass concentrations are described by log-normal distributions, and the remaining models

25   use the sectional approach with various numbers of monodisperse size-bins describing aerosol particle number concentration and chemical composition (Table S2).

Regarding the eight modal models, six of them (the three ECHAM models, EMAC, TM4-ECPL and TM5) are based on the M7 aerosol module developed by Vignati et al. (2004) for the description of aerosol microphysics, or improved versions of M7 to account for SO_2 oxidation to sulfuric acid, contribution of organics to growth, and additional aerosol species. Other

30   aerosol microphysics modules used in models participating in this study are the Model Aerosol Modules (MAM3 and MAM4; (Liu et al., 2012; Liu et al., 2016), the Advanced Particle Microphysics (APM) package (Yu and Luo, 2009; Yu, 2011; Yu et al., 2018), the TwO-Moment Aerosol Sectional (TOMAS) microphysics package (Adams and Seinfeld, 2002), the Multiconfiguration Aerosol Tracker of mIXing state (MATRIX) module (e.g. Bauer et al., 2008), the Aerosol Two-

dimensional bin module for formation and Aging Simulation version 2 (ATRAS2; Matsui, 2017) and a production tagged module OsloAero5.3 used in combination with the offline microphysics scheme AeroTab5.3 (Kirkevåg et al., 2018). Further details are provided in supplementary section S1.

5   Relevant to this study are also differences in the aerosol components that are taken into consideration in the models for the CCN calculations. Nine models (CAM5- MAM3, CMA5-MAM4, CAM5-3-Oslo, the three ECHAM models, GEOS-Chem-TOMAS, GISS-E2-TOMAS models and TM4-ECPL) do not account for particulate nitrate at all or in the CCN calculations (supplementary Table S2). TM4-ECPL however computes NO_3^- and NH_4^+ mass distribution in fine and coarse modes by the ISORROPIA II module (Fountoukis and Nenes, 2007). Similarly TM5 uses EQSAM (Metzger et al., 2002b, 2002a) to calculate using bulk aerosol approach the partitioning of ammonium nitrate between gaseous and particulate phase
10 with the particulate mass assumed to reside in soluble accumulation mode. In addition, while all models account for in-cloud scavenging of aerosols and for the aerosol release from evaporation of droplets, a few models account for melting and sublimation of ice crystals. For the calculation of CCN concentrations from the aerosol number and mass distributions, models need to specify their hygroscopicity from the volume-weighted hygroscopicities of the each constituent (Table 1) following the approach of Petters and Kreidenweis (2007).

15 In addition to these 15 models, we include the results from perturbed parameter ensemble (PPE) simulations using HadGEM3-UKCA (Yoshioka et al., in-prep; see details in supplementary section S1). The PPE consists of 235 atmosphere-only simulations for the year 2008 with 26 parameters controlling aerosol emissions and processes perturbed simultaneously. Simulations were nudged to ERA-Interim wind and temperature and all aerosol feedbacks to atmospheric dynamics are turned off. Therefore all simulations share the same meteorology. CCN number concentrations were calculated globally for
20 all member simulations and taken at geographical locations and elevations of observation stations. These simulations were then used to create Gaussian process emulators at each station location from which 260,000 'model variants' were generated that densely sample the 26-dimension parameter space. The emulators were validated against additional model simulations to show that the emulator uncertainty is much smaller than the model parametric uncertainty.

2.2 Observational data for model evaluation

25 Datasets of CCN at various supersaturations, particle number concentrations, size distributions and particle chemical composition measured at one atmospheric monitoring station in Japan and eight Aerosols, Clouds, and Trace gases Research InfraStructure (ACTRIS) atmospheric monitoring stations in Europe (Schmale et al., 2017) were used in the present study (Figure 1) for evaluation of model results. The observatories are representative of different environments (Pacific, Atlantic and Mediterranean marine atmospheres, high alpine and boreal forest continental atmospheres). A brief site description of
30 the observatories is provided in the supplementary Table S4, while more technical details are given by Schmale et al. (2017). While in general measurement data are available from the period of 2011 to 2015, each station covered only a sub-period of those five years, but at least one entire year (Schmale et al., 2017). Despite using point measurements, the long period of observations allows evaluation of the global models without biases associated with the model resolution (Schutgens et al.,

2016). Six out of the nine stations provided non-refractory chemical composition data of submicron particles (based on aerosol mass spectrometry); while all stations recorded submicron particle number size distributions and CCN number concentrations over a variety of supersaturations. A detailed discussion of the observational results can be found in Schmale et al. (2018).

5   For this study, the observations of CCN concentrations at supersaturations spanning between 0.1 and 1.0%, the number concentrations of aerosols with dry diameters larger than 50, 80, and 120 nm (denoted hereafter as N_{50}, N_{80}, N_{120}, respectively), as well as PM_1 (particles with dry diameters less than 1 μm) chemical composition (mainly sulfate (SO_4^{2-} hereafter SO4), organic aerosol (OA)) from the nine stations are used. The CCN data for these stations cover at least 75% of each year (Schmale et al., 2017). Observational data have been further filtered so that there is a minimum data requirement,

10   which means that daily averages are calculated from hourly data only for days with at least six hourly measurements. Monthly averages follow similar method, where the average is calculated only for months with at least 10 daily averages. When fewer data are available, the data are not considered representative of this quantity and are not included in the comparisons with the model results.

2.3 Design of the experiment

15 This model experiment has been designed within the BACCHUS EU project and has been opened for participation to the entire AEROCOM global modeling community. Global simulations have been performed for the years 2010-2015 (2010 is used as a spin-up). SO4, BC, OA, SS and DU are the aerosol components that are considered here. Models provided hourly values for the N_{50}, N_{80}, N_{120}; CCN number concentrations for thirteen supersaturations ranging from 0.05% up to 1.0% (that are 0.05%, 0.075%, 0.1%, 0.15% and from 0.2% to 1.0% in increments of 0.1%, denoted hereafter as CCN_i, where

20 i=supersaturation value); the chemical composition of PM_1 particles at the station locations (Table S4). The large number of different supersaturations at which CCN are computed allows for direct comparisons with all available observations of CCN for the nine stations as well as for the calculation of CDNC (Section 2.4). Among the models that participated in the present study GISS-E2-TOMAS and HadGEM3-UKCA did not provide any results for the stations due to meteorology not corresponding to the measurement time period (free-running for the first one and 2008 for the second); therefore, all multi-

25 model median (MMM) for the stations presented below have been computed excluding these models.

    Beyond station data, the global annual mean surface distribution of the $CCN_{0.2}$, the particle numbers N_3, N_{50}, N_{80} and N_{120} and the mass composition of the PM_1 particles for the year 2011 are provided by fifteen models (HadGEM3-UKCA did not provide such results). The MMM has been computed as the median of the contributing models.

    In addition to the data provided by the 15 global models, the results of the PPE using HadGEM3-UKCA (Yoshika et al,

30 in prep) are used in this study to quantify the model parametric uncertainty in CCN and to perform a sensitivity analysis to quantify how each parameter contributes to the overall uncertainty.

2.4 Data interpretation methodology

CCN Persistence. To investigate the duration for which the CCN number concentration remains similar to its earlier concentration, the autocorrelation function (ACF) of the CCN time series has been calculated as in Schmale et al. (2018) (see also supplementary S2). This ACF may provide valuable information about the drivers of the variability of the CCN number

5   concentration in the atmosphere. In the present study, we chose to compute the ACF based on model results of $CCN_{0.2}$ at the 9 sampling sites and compare them with the corresponding ACF obtained from observations (Schmale et al., 2018). For a direct comparison, we use the same time periods as for the observations, which vary among the sampling sites. For all ACF calculations, hourly data of $CCN_{0.2}$ were used, for both the observations and model results.

CDNC calculations. While GCMs calculate CDNC using a variety of approaches, for the present study CDNC is calculated

10   off-line, using a common parameterization for CCN spectra derived from the models or from the observations. This approach allows understanding the importance of differences in modeled and observed CCN spectra by expressing them as differences in CDNC that would form in a given type of cloud. We have calculated CDNC for two different updraft velocities: one characteristic for stratiform clouds ($w = 0.3\ \mathrm{ms}^{-1}$) and the second characteristic for cumulus clouds ($w = 0.6\ \mathrm{ms}^{-1}$). Similar calculations have been performed using the observed CCN spectra at the stations, where such information

15   is available, to enable comparison of model results with observations. The ability of the modeled CCN spectra to reproduce the observed sensitivity of CDNC to aerosol or to updraft velocity is also evaluated.

The calculation of CDNC is based on the parameterization of Nenes and Seinfeld (2003) with the mass transfer augmentations proposed by Fountoukis and Nenes (2005), Barahona and Nenes (2007) and Morales Betancourt and Nenes (2014). Using the CCN at different supersaturations (section 2.3) allows to consistently construct the CCN spectrum function

20   $F(s)$ from each simulation - which provides the CCN number as a function of supersaturation, s (Sotiropoulou et al., 2006):

$$F(s) = \frac{N}{1 + \left(\frac{s}{b}\right)^a} \qquad (2)$$

where N is the total number of particles, and a, b are parameters determined using a non-linear fitting procedure for each one of the participating models. $F(s)$ is then computed for each station's grid point and time step of the model outputs (with b and a being fitting parameters), and CDNC, denoted in the figures by N_d, is computed from the parameterization for prescribed values of the vertical velocity. This fitting approach has been also applied to the CCN observations since they are

25   available only for a limited number of supersaturations; and thus cannot be directly used for accurate calculation of CDNC. A well-constrained CCN spectrum requires concentrations for at least five different supersaturations at the same time instance (Sotiropoulou et al., 2006). Such information was available only at five stations (Cabauw, Finokalia, Jungfraujoch, Mace Head and Vavihill), which are subsequently used for deriving CDNC based on observations and compared against model-derived CDNC.

30   The CDNC parameterization uses as input $F(s)$, cloud-base pressure and temperature, and the vertical velocity characterizing the cloud updraft (either as a single updraft, or a "characteristic" value that provides a distribution-averaged

value; Morales and Nenes, 2010). It determines the value of maximum supersaturation, s_{max}, that develops in the cloudy updrafts, using the concept of "Population Splitting" (Nenes and Seinfeld, 2003). CDNC is then obtained from the CCN spectrum as $N_d=F(s_{max})$. This approach works well for stratus and stratocumulus clouds (Morales and Nenes, 2010). CDNC calculated here is from primary activation and does not consider the influence of pre-existing droplets, although

5   modifications to the parameterization can account for this as well (e.g., Barahona et al., 2014).

Ensemble modeling computation. The modeled hourly aerosol particle number concentrations, mass composition, CCN and CDNC at the nine stations have been used to calculate daily and monthly averages. Comparison of individual model results with observations is provided in the Supplementary Material Figures S2 and S3, because it can be used to identify strengths and weaknesses of each specific model and can serve as a guide for model improvements in the future. In Section 3, the

10   multi-model median (MMM) is compared to observations. The diversity of the model results (defined as the ratio of standard deviation-to-mean) and the mean of the models, which in several cases significantly differs from the MMM, are also reported in these comparisons.

Annual averages of the global surface distributions of N_3, N_{50}, N_{120}, $CCN_{0.2}$ and PM_1 mass concentrations of the major aerosol components have been provided by a total of fifteen models. Global fields have first been re-gridded to a $5°\times5°$ grid

15   for all models. Then the MMM and diversity are calculated, as described above, for the stations. Note that $5°\times5°$ is a very coarse grid size, which would no doubt affect the model-to-observations comparison, particularly when comparing to sites within small heavily polluted area where a large rural background is now also being added in and vice versa. Therefore, it is worth mentioning that the surface stations used for model comparison are representative of the larger area in which they are located and justify our choice for a relatively large grid to re-grid all model results. For the mountain stations, the appropriate

20   model level has been considered that corresponds to the station's altitude above sea level. Annual means of the individual models are also presented in the Supplementary Material (Figures S6 to S14).

3 Evaluation against station observations

3.1 CCN number concentrations comparisons with multi-model median

The models tend to underestimate the monthly $CCN_{0.2}$ number concentration in the lowest model level at all sites (Fig. 2

25   and supplementary Fig. S2) for the years 2011-2015: Average normalized mean bias (NMB) of all models and for the nine sites is as low as -36% and the normalized mean error (NME) is 69%; while among individual models and stations NMB and NME vary from -88% to +145% and from 40% to 159%, respectively (see supplementary section S3.2 for definitions and Table S5 for results). The Finokalia station is an exception, where most models overestimate $CCN_{0.2}$ (average NMB around 47%) with eight models showing significant overestimation (NMB>10%) and six models smaller deviations from

30   observations (-10%<NMB<10%). Among the studied locations, Finokalia is the station with the highest observed critical diameter (~200 nm at a supersaturation of 0.2% according to Schmale et al., 2018), therefore, potential inaccuracies in the model-determination of the critical size may be responsible for the model overestimate of $CCN_{0.2}$ at this station. The

underestimation of the observed CCN0.2 by the models is largest at the high alpine site of Jungfraujoch (mean NMB of all models: -73%), where none of the models is able to capture the maximum observed values of $CCN_{0.2}$ (~300-600 cm^{-3}) during summer. Deficiencies in the models' representation of the boundary layer and mixing of air between the boundary layer and the free troposphere in complex terrain like the Alps as well as the sampling of the models based on the station's

5   altitude might be reasons for this systematic underestimation by the models (D'Andrea et al., 2016). Despite the quantitative differences in the estimation of the $CCN_{0.2}$ concentrations, models are able to capture satisfactorily the relative differences in $CCN_{0.2}$ concentrations between stations, as well as their seasonal variations. The model-mean index-of-agreement (IoA, see definition in Supporting Material section S3.2) varies between 0.46 and 0.63 for the different stations with the best for Finokalia remote coastal station and the worst for Jungfraujoch alpine station. The largest difference in performance among

10   models is found for the Mace Head station with an IoA varying between 0.20 and 0.89 for the individual models (Table S5).

   To compare the calculated MMM and the observed seasonal variability of $CCN_{0.2}$ for each station (Fig. 3), the monthly model results have been temporally co-located with monthly mean observations. Furthermore, to increase clarity in Figure 3, for each station, the MMM $CCN_{0.2}$ has been multiplied by a scaling factor, f, so that the four season's mean of the simulated MMM $CCN_{0.2}$ concentrations becomes equal to the corresponding observed value. The factor f is denoted for each station

15   inside the frame. Overall, the seasonal pattern is nicely captured by the models, although the absolute values are underestimated everywhere ($f > 1.50$) except at Finokalia ($f=0.82$) as discussed earlier.

   For the high altitude continental background sites (Puy de Dôme, Jungfraujoch) low number concentrations with high seasonal variability are observed (winter (DJF) minimum and summer (JJA) maximum with observed ratios of summer-to-winter of 2.17 and 5.37, respectively, while the simulated MMM ratios are 3.19 and 5.58). This strong seasonality is

20   attributed to changes in the height of the boundary layer that can affect these sites during summer but not during winter when the sites are mostly in the free troposphere (Schmale et al., 2018). At Jungfraujoch the boundary layer virtually never reaches up to the site. Instead, increased concentrations are caused by injections of boundary layer air into the lower free troposphere over the mountainous terrain. The free tropospheric background concentration of CCN is very low such that increases in number concentration of CCN-sized particles (90 nm in diameter) are a good indicator for boundary layer

25   influence (Herrmann et al., 2015).

   On the other hand, high $CCN_{0.2}$ number concentrations but low seasonal variability is found for the rural background stations of Cabauw and Melpitz, indicative of the elevated air pollution background in these regions. At these stations highest $CCN_{0.2}$ number concentrations are observed during spring, which are underestimated by the MMM. Furthermore, observations show a monotonous decrease from spring to summer and fall, while models calculated high summertime values

30   than in spring and fall at Cabauw and a monotonous increase from spring to fall at Melpitz. This could indicate that the models are not following the observed changes in the aerosol particle number concentration and/or the critical diameter at these stations (Schmale et al., 2018), possibly also associated with the adopted sizes in the primary aerosol emissions at these locations. At the other rural background station (Vavihill), both models and observations show lower $CCN_{0.2}$

concentrations and seasonal variability than at Cabauw or Melpitz. In addition, observations indicate a higher critical diameter at Vavihill (around 120 nm) than at the other two stations (around 90 nm) (Schmale et al., 2018).

Different seasonal cycles are also observed among the three coastal sites Mace Head, Finokalia and the Noto Peninsula: At the Mace Head site, due to the clean marine conditions over the Atlantic Ocean (Ovadnevaite et al., 2014), low $CCN_{0.2}$

5   concentrations are observed through the year. There, the highest concentrations are observed and simulated during spring. Both Finokalia and Noto Peninsula are impacted by long range transport that occurs through the free troposphere and affects the surface by mixing down into the boundary layer and the models qualitatively reproduce the observed seasonal cycles, simulating a high variation in the number concentration over the year. At Finokalia the observed and simulated summer seasonal maximum is also attributed to biomass burning plumes from north-east Europe (Bougiatioti et al., 2016), while

10   high $CCN_{0.2}$ concentrations peaking in spring (observations available only for May) over the Noto Peninsula are due to pollutants originating from East Asia (Iwamoto et al., 2016, Schmale et al., 2018). However, the observed sharp decline of $CCN_{0.2}$ during the spring (May)-summer transition over the Noto Peninsula is also reproduced by the models. At Finokalia the models qualitatively follow the observed seasonality, although the observed summer-to-winter ratio (4.6) is underestimated by the models (2.3; Fig. 3). This can be due to the CCN sensitivity to loss by deposition during winter and to

15   OA formation and hygroscopicity during summer that combined weaken the simulated seasonality (further discussion in section 5).

Finally, at Hyytiälä, on average the models calculate relatively small $CCN_{0.2}$ number concentrations and a low seasonal variability with a maximum in concentrations in summer, in agreement with observations, although they slightly underestimate the observed summer-to-winter ratio (1.5 modeled versus 1.7 observed). As discussed further in section 5, at

20   Hyytiälä the modeled $CCN_{0.2}$ is very sensitive to errors in OA hygroscopicity and in secondary organic aerosol (SOA) formation from biogenic organic precursors during summer. Therefore, uncertainties in OA in the models and in particular underestimates of OA are expected to affect the summer-to-winter ratio.

Observed CCN number concentrations at the maximum supersaturation ratios measured at each station (which vary among stations, ranging from 0.7% to 1.0%) are compared to models in Figure 4. CCN at various supersaturation ratios

25   provides insights into the size distribution and the chemical composition in the models, since at high supersaturations small and less hygroscopic particles also activate. Most models underestimate CCN at high supersaturation at all stations with available observations (Figure 4), indicating that insufficient number of small particles activate in the models. However, observations are captured by the maximum and minimum of the 14 models (dashed green line) except for the alpine Jungfraujoch station. Overall, the average NMB and NME of all models and for the all stations with available observations

30   are -34% and 78% respectively; while among individual models and stations NMB varies from about -89 to about +253% (Table S5).

Comparing model performance for CCN at low supersaturation ($CCN_{0.2}$, Figure 2) and at high supersaturation ($CCN_{1.0}$, Figure 4), $CCN_{1.0}$ is systematically underestimated by the models across all stations, but the model and station average NME is about 15% higher for $CCN_{1.0}$ than for $CCN_{0.2}$, indicating that larger particles are better captured by the models than the

smaller ones (see also supplementary Table S5). The $CCN_{1.0}$ seasonal variability is predicted satisfactorily. Since the number concentration of CCN depends on both the chemical composition and the number of aerosol particles, it is worth investigating the role of these two factors separately.

3.2 CCN number concentrations comparisons with PPE

$CCN_{0.2}$ concentrations in perturbed parameter ensemble (PPE) simulations using HadGEM3-UKCA (Yoshioka et al., in-prep) for 2008 at these stations are shown in Figure 5, together with observations. The blue solid line shows the emulator mean, the blue shading the range of one standard deviation around the mean, and the dotted lines the minimum and maximum emulator values. The range of one standard deviation either side of the mean value represents approximately 68% of all samples, therefore the blue shading shows approximately the same relative range as for the multi-model comparison in Figure 2 (25%/75% quartiles). Different years of available observations are shown as stars, pluses and crosses respectively. Since the interannual variability of simulated MMM $CCN_{0.2}$ concentrations shown in Figure 2 is generally small compared to inter-model variability, the difference in years between simulations and observations is not considered to undermine the model-data comparisons.

Except for Mace Head, the uncertainty ranges in the PPE are somewhat smaller than the 25%/75% quartiles of the models shown in Figure 2. This suggests model structural differences and emission inventories used in different models are more important source of diversity of estimated $CCN_{0.2}$ concentrations for central 70% range than fully sampled parametric uncertainty in a single model. However, the maximum-minimum ranges are much larger in the PPE than in the MMM at many locations. Therefore, the emulator values from PPE are more concentrated near the mean but have longer tails compared to values from MMM. This is to be expected from such a relatively small sample of models in the MMM.

Model-data comparisons are qualitatively similar to the case with MMM. The PPE simulations underestimate the observed $CCN_{0.2}$ concentrations at many stations and months. Exceptions are Puy de Dome and Hyytiälä where PPE simulations reproduce the observations well for most of the months and Finokalia where, just like MMM, the PPE overestimates the observations. At Melpitz and Vavihill simulations capture the observed values in summer but underestimate them in winter and early spring. The PPE simulations fail to capture the observed peaks in winter and early spring at Mace Head and Cabauw as well. This is unlike the case with MMM which does not show a distinct winter time underestimate (Figure 3).

3.3 Particle number concentration and PM_1 aerosol chemical composition

The observed critical diameter for particle activation into CCN at 0.2% supersaturation at most of the locations in this study is around 100 nm or larger, reaching about 200 nm in spring and summer at Finokalia (Schmale et al., 2018). Therefore in Figure 6, the MMM of the simulated N_{50} and N_{120} are depicted together with the 25%/75% quartiles of all models that provided station data and are compared with observations. N_{120} is expected to represent a significant portion of

the activated particles at 0.2% or higher supersaturation. The models underestimate N_{50} and on average NMB is -24% and NME is 73% for all models and stations. N_{80} is not shown in this figure but follows a similar behavior as N_{50} and N_{120}. It is not surprising that in almost all cases both the N_{50} and the N_{120} concentrations are underestimated (the average NMB for all models and stations is -35% and the NME is 64%) by a factor that is slightly only lower than the underestimation of the

5    $CCN_{0.2}$ concentration (-36% NMB and +69% NME). It may therefore be concluded that the quantitative differences of the models in the prediction of CCN originate from the underestimation of the number concentration of aerosol particles in the relevant size ranges.

Figure S1, which is similar to Figures 2 and 4 but shows particulate SO4, OA mass in PM_1 particles at the nine stations as well as model results for DU and SS, reveals a reasonable agreement of the MMM with the corresponding available

10   observations where available (average NMB for all models and all stations is +38% for SO4 and -37% for OA and NME is 97% for SO4 and 75% for OA). Strong seasonal variations of the SO4 mass of about one order of magnitude are observed and simulated at the coastal background stations, Mace Head and Finokalia, and at the alpine site, Jungfraujoch. A smaller seasonal variation of SO4 is observed at the boreal forest environment of Hyytiälä and at the rural background station Cabauw, while at the highly polluted Melpitz station no significant seasonal pattern of the SO4 mass is observed during the

15   year. At these three stations, the MMM captures the observed annual mean concentration of SO4, but fails to reproduce the seasonality. Strong seasonal variations of the OA mass are observed and simulated at Mace Head, Finokalia, Jungfraujoch and Hyytiälä, while no distinct seasonal cycle in organic mass is seen at Cabauw and Melpitz. The IoA between the MMM and the observations is between 0.28 and 0.62 for all stations. A detailed analysis of each model separately (Supplementary Table S5) shows that the OA mass concentration is underestimated (mean NMB is -37% by the nine of the models and

20   overestimated by six of them and not systematically the same models at all stations (range of NMB -97% to 216%). Because different models are appearing as outliers at each station, it is difficult to conclude whether the parameterizations in one model are better than another. This, however, is consistent with the findings of a recent OA intercomparison study that considered 31 models (Tsigaridis et al., 2014) and several modeling studies that suggest a missing source of OA needed to reconcile observations with model results (Spracklen et al., 2011a; Heald et al., 2011). It appears therefore that in addition to

25   the aerosol number concentration earlier discussed, a possible source of error in the simulation of aerosol and CCN number concentrations in the present study originates from the underestimation of the submicron OA mass at the stations where significant contribution of the submicron OA mass to the $CCN_{0.2}$ levels has been observed (Schmale et al., 2018). The importance contribution of OA in the uncertainty of CCN is also supported by the PPE simulations further discussed in section 5.

30   **3.4 CCN persistence**

The above analysis of CCN and aerosol number concentrations shows that on average the models are able to simulate the seasonal variations in CCN concentrations; while the model-to-observation differences in the CCN concentrations can be attributed mainly to a systematic underestimation of the number of aerosol particles that are large enough to act as CCN. The

ability of models to simulate short-term variations (order of days) of the CCN number concentration is examined based on the calculated persistence of $CCN_{0.2}$ number concentrations during summer and winter (see section 2.4) for all stations and for each model. The average persistence times for all models are compared in Figure 7 with those derived from the observations (Schmale et al., 2018). Depending on the season and the station, the persistence time varies from a few hours

5 (e.g., summer in Mace Head) to several days (e.g., winter in Melpitz).

Depending on the station, the persistence time is longer during winter or during summer. The average persistence of the $CCN_{0.2}$ number concentrations simulated by the individual models qualitatively captures the observed relative change of the persistence between winter and summer. The models show much smaller ratio than the observations at most of the stations except at Mace Head, Noto Peninsula and Vavihill where the ratio is opposite. For the high-altitude stations, Puy de Dôme

10 and Jungfraujoch, the models calculate longer persistence times during summer than during winter, in agreement with the observations. For these two high-altitude stations, a significant increase in the number concentration of $CCN_{0.2}$ is observed during summer, because the stations are subjected to the boundary layer air mass influence during that season, while during winter they are largely in the free troposphere. Therefore, despite the fact that the number concentration of $CCN_{0.2}$ is overall underestimated, the models are able to reproduce the dynamical behavior of these continental background stations, most

15 probably because they are able to simulate the local meteorological changes that drive CCN persistence (supplementary Figure S4 and further discussion in supplementary section S3.1).

Analyzing the reasons that affect the persistence and then attributing the differences between the observed and the model-derived values to the underlying physical and/or chemical process parameterizations in each model is a demanding task which is also likely to be model and case dependent. In addition to atmospheric transport patterns, wet deposition is

20 presumably affecting the persistence time, however, this exercise, not focusing on wet deposition of aerosols, does not have the necessary elements to elaborate this issue. Furthermore, the size of the emitted OA and BC particles has been shown to be an important parameter to which the persistence time and in particular the summer-to-winter ratio of CCN is sensitive (see sensitivity runs performed with one (TM4-ECPL) among the participating models in the supplementary material, supplementary section S3.1 and Figure S5). Section 5 further attributes $CCN_{0.2}$ uncertainty to various parameters.

3.5 Cloud droplet number concentration from CCN spectra

Inside a cloudy updraft, s_{max} is reached when supersaturation generation from expansion cooling becomes equal to its depletion by the condensation of water vapor onto the growing droplets (Nenes and Seinfeld, 2003). Increasing updraft velocity enhances the cooling rate of the cloudy air parcels, which in turn allows higher supersaturation and eventually

30 increases s_{max} and CDNC (N_d in the following text and figures). Increases in CCN concentrations tend to increase N_d and associated water vapor depletion in the early stages of cloud formation; this in turn hinders the development of supersaturation and eventual decrease in s_{max}. This water vapor "competition effect" is especially strong when clouds form in the presence of large, hygroscopic particles such as sea-salt aerosol or large amounts of accumulation aerosol (Morales

Betancourt and Nenes, 2014; Ghan et al., 1998). Competition effects in turn explain why droplet number responses exhibit a sublinear response to modulations in CCN; only when CCN concentrations are very low (or updraft velocities very high), s_{max} becomes high enough so that the sensitivity of N_d to CCN approaches unity.

Based on the behavior described above, one can understand the N_d predicted from simulated and observed CCN spectra. As expected, both s_{max} values and N_d for all observations and simulations are higher for $w = 0.6\ ms^{-1}$ than for $w = 0.3\ ms^{-1}$. The response of s_{max} and N_d to increasing w also depends on the activated fraction (Fig. 8 third row). The calculated N_d increases progressively from the low values seen for the clean marine conditions at Mace Head and the high alpine atmospheric conditions of Jungfraujoch to the rural background conditions at Cabauw and Vavihill; while at Finokalia the observationally derived N_d are the largest among the five stations (Fig. 9a) and higher than at Cabauw. At Jungfraujoch, Finokalia and Mace Head, the seasonal variability of N_d is captured, despite the fact that the multi-model median tends to underestimate the observationally derived N_d. However, the individual models show both over- or under- predictions of the observations (supplementary Fig. S3). Owing to the water vapour competition effect, s_{max} decreases for increasing N_d, meaning that clouds at a given location do not have a "characteristic s_{max}", but rather depends on the given set of aerosol and dynamical conditions active during the cloud formation.

For all stations except Finokalia and Jungfraujoch, the agreement between the model and observationally derived N_d (Fig. 8) tends to be better than for CCN (Fig. 2, 4) and aerosol number concentrations (Fig. 6) (as expressed by the model-mean NMB for all stations provided in Table S5). This trend is a result of the competition effect of CCN on s_{max}; if observed CCN concentrations are higher than predicted, then the "observed" s_{max} tend to be less than the "predicted" s_{max} - which means the discrepancy in "observed" and "predicted" N_d is reduced compared to the CCN errors. The error reduction is substantial, especially under lower updraft velocity conditions. As qualitative example we here present the ratio of the observed to the simulated average values of $CCN_{0.2}$ number concentrations that is 4.0 at Jungfraujoch, 2.2 at Cabauw, 2.1 at Mace Head, 1.5 at Vavihill, and 0.8 at Finokalia (Fig. 3). In the case of N_d the corresponding ratios for $w=0.6$ m.s^{-1} are ~1.8 at Jungfraujoch, ~0.9 at Cabauw, ~1.5 at Mace Head, ~0.9 at Vavihill and ~1.8 at Finokalia (Fig. 9). All these ratios are inversely correlated with the observed to the simulated average values of s_{max} (Fig. 9), a clear indication of competition effects on N_d and prediction error mitigation.

These results clearly indicate that the number of CCN at a prescribed supersaturation cannot be used as an indicator for the number of activated droplets, as supersaturation is dynamically determined and can vary considerably for a given site. CCN-derived comparisons cannot even be used qualitatively, as the supersaturation levels can be so different from a prescribed value that even the error trend in N_d may not be reflected. For example, according to observationally derived data, $CCN_{0.2}$ at Cabauw is significantly higher than at Finokalia, although at Finokalia N_d is larger for the observations but not for the model results. Our analysis however clearly shows that the models examined here do not exhibit the same level of N_d prediction error as CCN error– a robust trend which is a result of the physics of cloud droplet formation.

4 Global distributions of surface $CCN_{0.2}$ and particle number concentrations

The global near-surface annual mean MMM distributions of the N_3, N_{50} and $CCN_{0.2}$ number concentrations for the year 2011 (Fig. 10) show similar patterns, i.e. larger concentrations over the continents due to the primary anthropogenic emissions over industrialized areas in USA, Europe, and Asia, and dust and biomass burning emissions in the tropics.

5   Multi-model median near surface N_3 number concentrations over continental regions vary between 1,000-10,600 cm^{-3}, while over the marine boundary layer (MBL) they vary between 100-2,000 cm^{-3}, rarely exceeding 300 cm^{-3} (Fig. 10a). The MMM N_3 surface distribution is similar to the results by Spracklen et al. (2010) and Gordon et al. (2017), who computed maximum N_3 concentrations of ~10,000 cm^{-3}. The concentration of N_3 is directly related to new particle formation and growth as well as to primary emitted particles. Since models use different nucleation mechanisms and emission inventories it

10   is expected that the diversity of the model results is higher for N_3 than for particle number concentration with larger (low-end) cut-off diameter. The largest diversities in the model results (Fig. 10b) are found in the Polar regions, where concentrations are relatively low, and in the continental boundary layer with high values (about 2) observed in the tropics and particularly in South America and over the boreal regions in Asia. Diversities of up to 1.5 are computed for the Mediterranean, Arabian Peninsula, Central Africa, Indonesia and South East Asia, indicating differences between models in

15   the representation of primary and secondary aerosol sources in these regions. Over the oceans the diversity is lower (<1) except in the high latitudes of the Northern Hemisphere where it exceeds 1.5. Even lower model diversity (around 0.8) is found in highly polluted areas over North America and Europe indicating consistency between models, in the representation of aerosols in these regions. In addition to new particle formation, our results point mainly to biomass burning emissions as major source of uncertainty in the model calculations resulting in high model divergence in areas like southern Europe,

20   tropical Africa and America, Southern Asia and Indonesia. Assumption of emission injection height is also a source of discrepancy between models (Daskalakis et al., 2015). The highest maximum N_3 concentrations in a $5^{o}x5^{o}$ grid box (supplementary Figure S6) were computed by the GISS-E2.1-MATRIX model (~176,000 cm^{-3}) and the TM4-ECPL model (~102,000 cm^{-3}) while the lowest were from the ECHAM6_HAM2-AP model (~6,400 cm^{-3}). A sensitivity simulation was performed by a single model (TM4-ECPL; discussed in sect. 3.3 and supplementary section S3.1 and Figure S5) assuming

25   the same primary emissions of carbonaceous aerosol in terms of mass to be emitted at larger particle sizes. This additional simulation shows the importance of the assumptions on size distribution of the emissions in the models since the results of this simulation are very close to the average of the other models. In agreement with these findings, Spracklen et al. (2010) concluded that the sensitivity of N_3 to the size of emitted particles originating from anthropogenic activities is significantly higher in regions close to anthropogenic sources and significantly lower at the remote boundary layer sites.

30   The annual global mean distribution of near-surface N_{50} particle number concentrations, (Fig. 10c) is similar to that of the N_3 particles, but the number concentrations are lower for these larger particle sizes that are more relevant for CCN. The spatial distributions of N_{50} are similar, but their concentrations are reduced by about a factor of 2.5 compared to N_3. The highest values of N_{50} are found over or close to industrialized regions due to anthropogenic emissions, and over Central

Africa and South America due to strong biomass burning emissions. Over marine regions, N_{50} is higher in the Northern Hemisphere than in the Southern Hemisphere due to the outflow from continental anthropogenic sources. Despite the similarities of the global MMM distributions, the models' diversity and spatial pattern of N_{50} (Fig. 10d) differ significantly from that of N_3. Excluding polar regions as for N_3, the highest model diversities for N_{50} (~2) are observed in regions with strong biomass burning emissions (Southern America, Central Africa and Indonesia) and high diversities are also found over the tropical Pacific which might be associated with marine emissions representation in the models. In all other regions the diversity of N_{50} simulations does not exceed 1, even over the remaining tropical and southern oceans, where sea salt is important.

The near surface MMM concentrations of the $CCN_{0.2}$ do not exceed 3,500 cm^{-3} over polluted areas in Europe, Asia and the United States, as shown in Fig. 10e. This value is significantly lower than the $CCN_{0.2}$ concentrations simulated by Spracklen et al. (2011) of up to 10,000 cm^{-3}. In the present study, only one model (EMAC) computes $CCN_{0.2}$ levels that exceed 10,000 cm^{-3} over the Taklimakan desert in Asia, while the remaining fourteen models show maximum surface $CCN_{0.2}$ concentrations < 5,000 cm^{-3} (see supplementary Figure S9). The surface distribution and magnitude of $CCN_{0.2}$ is similar to N_{120} (supplementary Figure S8) with the maximum $CCN_{0.2}$ concentrations only slightly lower than the N_{120} values for most models, indicating that most of the N_{120} particles activate, implying a global-mean kappa of ~0.2 for 120 nm particles. However, analysis of the individual model results over the polluted areas shows that the number concentration of N_{120} can, in most cases, be either 50% lower or higher than that of $CCN_{0.2}$. The modeled $CCN_{0.2}$ diversity is lower than the diversity for N_{50} with values < 0.5 for mid-latitude continental regions and around 1 over the tropical oceans, where the $CCN_{0.2}$ number concentration is usually lower than 60 cm^{-3}, but also over the tropical S Africa and Central Africa where $CCN_{0.2}$ number concentration is a few hundreds of cm^{-3}.

Some of the differences in global near surface distributions of CCN (Fig. S9) can be associated with the corresponding differences in the computed SO4 and OA surface distributions (Fig. S10 and Fig. S11, respectively). For instance, in China and S. America, models that are biased low in SO4 and high in OA are also biased low in CCN. Significant differences are also found for black carbon, sea-salt and dust PM$_1$ components (Fig. S12-S14). The global surface distributions of the MMM of the chemical compound (SO4, BC, OA, SS and DU) concentrations that contribute to PM$_1$ are shown in the supplementary Figure S15 (left column) together with the corresponding model diversities (right column). For all simulated PM$_1$ components diversities maximize south of 60°S and north of 60°N, similarly to N_3, which reflects the challenges of the models in simulating atmospheric transport, deposition and chemistry close to the poles.

5. Causes of uncertainty in CCN

In this section we use the HadGEM-UKCA perturbed parameter ensemble (PPE) to identify some potential causes of model diversity and bias compared to the observations. We performed a variance-based sensitivity analysis at each measurement

site using the 260,000 HadGEM-UKCA model variants sampled from the emulator following the methodology described in previous studies (Lee et al., 2013; Johnson et al., 2018).

Figure 11 shows the fraction of variance in $CCN_{0.2}$ that can be attributed to each of the perturbed parameters. Here we draw attention to the main parameter effects and refer to Yoshioka et al. (in prep) for a full description of all parameters. In the summer, the largest contributions to uncertainty in $CCN_{0.2}$ at most sites are the biogenic volatile organic compounds (BVOC) emission flux and the assumed hygroscopicity of the organic matter in the particles (κ_{OA}). The BVOC emissions in this model are assumed to be α-pinene and to have an uncertainty range of 12-225 Tg SOA production per year. The κ_{OA} is assumed to have a range of 0.1-0.6 and to be fixed during the simulation time (i.e., the hygroscopicity does not change due to within-particle oxidation). Together, these two mostly biogenic-related parameters account for up to 90% of the CCN variance in summer, ranging from about 0% at Mace Head, 20% at Cabauw, 40% at Finokalia, 70% at Melpitz and 90% at Hyytiala. Except at the Mace Head coastal site, the other important parameters in summer are dry deposition of aerosol, anthropogenic SO_2 emissions (at Finokalia, Puy de Dome and Jungfraujoch), the fossil fuel emission flux (at Noto Peninsula, Cabauw and Melpitz), and the assumed width of the accumulation mode (at Jungfraujoch and Puy de Dome).

In winter, aerosol dry deposition is an important cause of uncertainty in $CCN_{0.2}$ at all sites except Jungfraujoch and Puy de Dome. At most sites (except Mace Head and Noto Peninsula) the emissions fluxes (and the assumed particle sizes) of carbonaceous aerosol from fossil fuel and residential combustion sources account for 10-20% of the uncertainty. Ageing of aerosol through uptake of sulphuric acid and SOA is also important at these sites. Finally, the production of sulphate through in-cloud oxidation by ozone accounts for 30-40% of the uncertainty at Finokalia, Puy de Dome and Jungfraujoch.

In summary, the PPE results suggest that production of SOA from biogenic emissions combined with the hygroscopic properties of the OA should in future be investigated as a source of differences between models in summer. In winter, dry deposition, ageing and in-cloud sulphate production are the dominant sources of uncertainty.

6 Summary and conclusions

Within the BACCHUS/AEROCOM multi-model CCN intercomparison initiative, a total of 16 global aerosol-climate and chemistry-transport models have compared to each other and to observations. Among them 14 provided results for particle and CCN number concentrations and PM_1 component mass concentrations, which have been compared to surface observations at eight sites in Europe and one in Japan to evaluate the skill of the simulations.

In this inter-model comparison, models used different meteorology and emissions (CMIP5/6 etc.) datasets/parameterizations. In general, most models and in particular the multi-model median underestimate the observed aerosol number concentrations N_{50}, N_{80} and N_{120}, as well as the CCN concentrations, suggesting incomplete understanding of the underlying processes. The models are, however, reproducing reasonably well the seasonal variability of N_{50}, N_{80}, N_{120}, and $CCN_{0.2}$ number concentrations, and SO4 and OA PM_1 component mass concentrations. While there are model

improvements since the 2014 AEROCOM organic aerosol intercomparison (Tsigaridis et al., 2014), most of the models continue to underestimate the organic submicron aerosol mass concentrations or to misrepresent the OA seasonal cycle.

The simulated N_3 number concentrations, which are generally higher over land, show high diversity among models over the Northern Hemisphere continents, while the simulated CCN are less diverse. This finding points to differences in the size

5   distribution of the primary emissions and/or in the formation and growth of new particles as important sources of the inter-model diversity in CCN.

CCN number concentrations are underestimated at all supersaturations by the MMM by at least 34% (Figure 9, Table S5). There is no model that performs best at all stations. The models on average qualitatively capture the strong seasonal variabilities of CCN observed at Finokalia, Noto Peninsula, Puy de Dôme and Jungfraujoch, and the very weak seasonality

10   observed at the other stations. Production of SOA from biogenic emissions combined with the hygroscopic properties of the OA in summer and dry deposition, ageing and in-cloud sulphate production in winter have been identified by PPE simulations as dominant sources of CCN uncertainty and should in future be investigated.

The short-term variability of $CCN_{0.2}$ at the measurement sites has been examined by comparing the $CCN_{0.2}$ persistence time computed from the observed data and the model results. Persistence is more sensitive to air masses changes and the

15   formation and removal rates of particles in the atmosphere than to the exact number concentration of CCN. The modeled persistence times of near-surface $CCN_{0.2}$ are between 0.5 and 16 days depending on the model, location and season. At 6 out of 9 stations the average relative change in modeled persistence time between winter and summer is in agreement with observations. These persistence times of $CCN_{0.2}$ are shown to be sensitive to assumptions on size of the emitted particles by a sensitivity simulation with TM4-ECPL model.

20   It is worth emphasizing that this is the first comparison of ensemble global aerosol climate model near-surface results with experimentally derived CDNC from surface measurements of CCN at different levels of supersaturation. Note that CDNC is not calculated by each participating model but a common methodology has been followed to derive the CDNC from the modeled and observed CCN spectra. Despite the large differences between models and observations found in the number concentration of aerosol particles and CCN, the CDNC estimates based on the CCN spectra are in significantly

25   better agreement than the CCN for the stations examined here. In addition, the inter-model spread of CDNC is smaller than that of particle and CCN number concentrations. These trends are robust and a result of the physics of cloud droplet response to aerosol perturbations.

As for CCN number concentrations, in several cases models underestimate CDNC when compared to the observationally derived CDNC (section 3.5). At high aerosol number concentrations, the maximum supersaturation is

30   computed to be small, limiting the fraction of particles that can activate and form CDNC. As a result, the sensitivity of CDNC to updraft velocity prevails. On the contrary, at high updraft velocities, CDNC is controlled by the variability in the aerosol number concentration. An anticorrelation is found between the sensitivity of CDNC to the number of aerosols and that to the updraft velocity, showing that the variability of these two parameters can explain the variability in CDNC and limit CDNC formation.

Our results are in agreement with previous studies showing that CDNC are sensitive to the uncertainties in the CCN number concentrations mainly in regions where aerosol number concentrations are low. Unlike previous studies, however, we show that for a large number of models, persistent and substantial CCN prediction biases are considerably reduced when expressed as droplet number concentrations for boundary layer-type clouds. We also find that model-observation comparisons of CCN at a prescribed supersaturation may be misleading in the error evaluation for CDNC, since supersaturation is dynamically determined and can vary considerably for a given site. The methodology proposed here, however, overcomes this limitation and considers the dynamic nature of supersaturation adjustment to CCN variations thus determining appropriate supersaturation levels for model-observation comparison. Such methodology can help better guide modeling efforts to focus on regions where CDNC predictions are most biased and sensitive to CCN perturbations (e.g., in the Southern Oceans).

Acknowledgements. This work has been supported by the European Union's Seventh Framework Programme (FP7/2007-2013) collaborative project BACCHUS (Impact of Biogenic versus Anthropogenic emissions on Clouds and Climate: towards a Holistic UnderStanding under grant agreement 603445. AN acknowledges support from the project PyroTRACH (ERC-2016-COG) funded from H2020-EU.1.1. - Excellent Science - European Research Council (ERC), project ID 726165. TB and TvN acknowledge funding from the European Union's Horizon 2020 research and innovation programme under grant agreement No 641816 (CRESCENDO) for their contributions to this study. The development of NorESM1 has been supported by the Norwegian Research Council through the projects EarthClim (207711/E10), EVA (grant no. 229771), the NOTUR (nn2345k) and NorStore (ns2345k) projects, and through the Nordic Centre of Excellence eSTICC (57001) and the EU H2020 project CRESCENDO (Grant no. 641816). PS also acknowledges funding from the European Research Council project RECAP under the European Union's Horizon 2020 research and innovation programme with grant agreement 724602. DWP acknowledges funding from Natural Environment Research Council project NE/L01355X/1 (CLARIFY). The ECHAM-HAMMOZ model is developed by a consortium composed of ETH Zurich, the Max Planck Institut für Meteorologie, Forschungszentrum Jülich, the University of Oxford, the Finnish Meteorological Institute and the Leibniz Institute for Tropospheric Research, and managed by the Center for Climate Systems Modeling (C2SM) at ETH Zurich. The computing time for this work was supported by a grant from the Swiss National Supercomputing Centre (CSCS) under project ID s652. HM acknowledges funding from the Japan Society for the Promotion of Science (JSPS), the Ministry of Education, Culture, Sports, Science, and Technology and the Japan Society for the Promotion of Science (MEXT/JSPS) KAKENHI Grant Numbers JP26740014, JP17H04709, JP26241003, and JP16H01770, MEXT Green Network of Excellence (GRENE) and Arctic Challenge for Sustainability (ArCS) projects, and the Environment Research and Technology Development Fund (2-1403, 2-1703) of Environmental Restoration and Conservation Agency. HW and YY acknowledge support from the U.S. Department of Energy (DOE), Office of Science, Biological and Environmental Research as part of the Earth System Modeling program. The Pacific Northwest National Laboratory (PNNL) is operated for DOE by Battelle

Memorial Institute under contract DE-AC05-76RLO1830. The CAM5-MAM3 simulation was performed using PNNL Institutional Computing resources. JK and JP were funded by the U.S. National Science Foundation, Atmospheric Chemistry Program, under Grant No. AGS-1559607 and the U.S National Oceanic and Atmospheric Administration, an Office of Science, Office of Atmospheric Chemistry, Carbon Cycle, and Climate Program, under the cooperative agreement award

5   #NA17OAR430001. GL and FY acknowledge support from NASA under grant NNX13AK20G and NSF under grant 1550816. SEB and KT acknowledges funding from NASA's Atmospheric Composition Modeling and Analysis Program (ACMAP), contract number NNX15AE36G. Resources supporting this work were provided by the NASA High-End Computing (HEC) Program through the NASA Center for Climate Simulation (NCCS) at Goddard Space Flight Center. MG acknowledges support from the ACTRIS2 project, EU H2020-INFRAIA-2014-2015, grant agreement no. 654109, the Swiss

10   State Secretariat for Education, Research and Innovation (SERI) under contract number 15.0159-1, and MeteoSwiss in the framework of the Swiss contributions (GAW-CH and GAW-CH-Plus) to the Global Atmosphere Watch programme of the World Meteorological Organization (WMO). This work has been finalized when MK was visiting L. Gallardo at the Center for Climate and Resilience Research (CR2) at the Geophysics Department of the University of Chile where MK profited from fruitful discussions.

Data availability

15   Currently the data used for this study are available upon request. After publication, they will be made available through a depository.

Authors contributions

GF performed TM4-ECPL model simulations, developed codes and has drawn all figures for the multi-model data analysis.

20   MK initiated and coordinated the exercise. AN developed the codes to interpret the CCN spectra from all models, the observations and performed CDNC calculations. MK and AN defined the experimental protocol. GF, MK, AN analyzed data and wrote the manuscript. All co-authors have contributed data and to the writing of the manuscript.

References

25   Abdul Razzak, H. and Ghan, S. J.: A parameterization of aerosol activation: 2. Multiple aerosol types, J Geophys Res. Atmos., 105(D5), 6837–6844, doi:10.1029/1999JD901161, 2000.
Adams, P. J. and Seinfeld, J. H.: Predicting global aerosol size distributions in general circulation models, J. Geophys. Res. Atmos., 107(19), 1–23, doi:10.1029/2001JD001010, 2002.
Barahona, D. and Nenes, A.: Parameterization of cloud droplet formation in large-scale models: Including effects of
30   entrainment, J. Geophys. Res. Atmos., 112(16), 1–14, doi:10.1029/2007JD008473, 2007.
Barahona, D., Molod, A., Bacmeister, J., Nenes, A., Gettelman, A., Morrison, H., Phillips, V. and Eichmann, A.:

Development of Two-Moment Cloud Microphysics for Liquid and Ice within the NASA Goddard Earth Observing System Model (GEOS-5), Geosci.Mod.Dev, 7, 1733–1766, 2014.

Bauer, S. E., Wright, D. L., Koch, D., Lewis, E. R., McGraw, R., Chang, L.-S., Schwartz, S. E. and Ruedy, R.: MATRIX (Multiconfiguration Aerosol TRacker of mIXing state): an aerosol microphysical module for global atmospheric models, Atmos. Chem. Phys., 8(20), 6003–6035, doi:10.5194/acp-8-6003-2008, 2008.

Bian, H., Chin, M., Hauglustaine, D. A., Schulz, M., Myhre, G., Bauer, S. E., Lund, M. T., Karydis, V. A., Kucsera, T. L., Pan, X., Pozzer, A., Skeie, R. B., Steenrod, S. D., Sudo, K., Tsigaridis, K., Tsimpidi, A. P. and Tsyro, S. G.: Investigation of global particulate nitrate from the AeroCom phase III experiment, Atmos. Chem. Phys., 17(21), 12911–12940, doi:10.5194/acp-17-12911-2017, 2017.

Boucher, O., Randall, D., Artaxo, P., Bretherton, C., Feingold, G., Forster, P., Kerminen, V.-M., Kondo, Y., Liao, H., Lohmann, U., Rasch, P., Satheesh, S. K., Sherwood, S., Stevens, B. and Zhang, X. Y.: Clouds and Aerosols, in Climate Change 2013 - The Physical Science Basis, edited by Intergovernmental Panel on Climate Change, pp. 571–658, Cambridge University Press, Cambridge., 2013.

Bougiatioti, A., Fountoukis, C., Kalivitis, N., Pandis, S. N., Nenes, A. and Mihalopoulos, N.: Cloud condensation nuclei measurements in the marine boundary layer of the Eastern Mediterranean: CCN closure and droplet growth kinetics, Atmos. Chem. Phys., 9(18), 7053–7066, doi:10.5194/acp-9-7053-2009, 2009.

Bougiatioti, A., Bezantakos, S., Stavroulas, I., Kalivitis, N., Kokkalis, P., Biskos, G., Mihalopoulos, N., Papayannis, A. and Nenes, A.: Biomass-burning impact on CCN number, hygroscopicity and cloud formation during summertime in the eastern Mediterranean, Atmos. Chem. Phys., 16(11), 7389–7409, doi:10.5194/acp-16-7389-2016, 2016.

Cubison, M. J., Ervens, B., Feingold, G., Docherty, K. S., Ulbrich, I. M., Shields, L., Prather, K., Hering, S. and Jimenez, J. L.: The influence of chemical composition and mixing state of Los Angeles urban aerosol on CCN number and cloud properties, Atmos. Chem. Phys., 8(18), 5649–5667, doi:10.5194/acpd-8-5629-2008, 2008.

D'Andrea, S. D., Häkkinen, S. A. K., Westervelt, D. M., Kuang, C., Levin, E. J. T., Kanawade, V. P., Leaitch, W. R., Spracklen, D. V., Riipinen, I. and Pierce, J. R.: Understanding global secondary organic aerosol amount and size-resolved condensational behavior, Atmos. Chem. Phys., 13(22), 11519–11534, doi:10.5194/acp-13-11519-2013, 2013.

D'Andrea, S. D., Ng, J. Y., Kodros, J. K., Atwood, S. A., Wheeler, M. J., Macdonald, A. M., Leaitch, W. R. and Pierce, J. R.: Source attribution of aerosol size distributions and model evaluation using Whistler Mountain measurements and GEOS-Chem-TOMAS simulations, Atmos. Chem. Phys., 16(1), 383–396, doi:10.5194/acp-16-383-2016, 2016.

Daskalakis, N., Myriokefalitakis, S. and Kanakidou, M.: Sensitivity of tropospheric loads and lifetimes of short lived pollutants to fire emissions, Atmos. Chem. Phys., 15(6), 3543–3563, doi:10.5194/acp-15-3543-2015, 2015.

DeMott, P. J., Prenni, A. J., Liu, X., Kreidenweis, S. M., Petters, M. D., Twohy, C. H., Richardson, M. S., Eidhammer, T. and Rogers, D. C.: Predicting global atmospheric ice nuclei distributions and their impacts on climate, Proc. Natl. Acad. Sci., 107(25), 11217–11222, doi:10.1073/pnas.0910818107, 2010.

DeMott, P. J., Hill, T. C. J., McCluskey, C. S., Prather, K. A., Collins, D. B., Sullivan, R. C., Ruppel, M. J., Mason, R. H., Irish, V. E., Lee, T., Hwang, C. Y., Rhee, T. S., Snider, J. R., McMeeking, G. R., Dhaniyala, S., Lewis, E. R., Wentzell, J. J. B., Abbatt, J., Lee, C., Sultana, C. M., Ault, A. P., Axson, J. L., Diaz Martinez, M., Venero, I., Santos-Figueroa, G., Stokes, M. D., Deane, G. B., Mayol-Bracero, O. L., Grassian, V. H., Bertram, T. H., Bertram, A. K., Moffett, B. F. and Franc, G. D.: Sea spray aerosol as a unique source of ice nucleating particles, Proc. Natl. Acad. Sci., 113(21), 5797–5803, doi:10.1073/pnas.1514034112, 2016.

Dusek, U., Frank, G. P., Hildebrandt, L., Curtius, J., Schneider, J., Walter, S., Chand, D., Drewnick, F., Hings, S., Jung, D., Borrmann, S. and Andreae, M. O.: Size Matters More Than Chemistry Aerosol Particles, Science (80-.)., 312(5778), 1375–1378, doi:10.1126/science.1125261, 2006.

Ervens, B., Cubison, M. J., Andrews, E., Feingold, G., Ogren, J. A., Jimenez, J. L., Quinn, P. K., Bates, T. S., Wang, J., Zhang, Q., Coe, H., Flynn, M. and Allan, J. D.: CCN predictions using simplified assumptions of organic aerosol composition and mixing state: A synthesis from six different locations, Atmos. Chem. Phys., 10(10), 4795–4807, doi:10.5194/acp-10-4795-2010, 2010.

Fan, J., Wang, Y., Rosenfeld, D., Liu, X., Fan, J., Wang, Y., Rosenfeld, D. and Liu, X.: Review of Aerosol–Cloud Interactions: Mechanisms, Significance, and Challenges, J. Atmos. Sci., 73(11), 4221–4252, doi:10.1175/JAS-D-16-0037.1, 2016.

Fountoukis, C. and Nenes, A.: Continued development of a cloud droplet formation parameterization for global climate

models, J. Geophys. Res. D Atmos., 110(11), 1–10, doi:10.1029/2004JD005591, 2005.

Fountoukis, C. and Nenes, A.: ISORROPIA II: a computationally efficient thermodynamic equilibrium model for K+– Ca2+–Mg2+–NH4+–Na+–SO42−–NO3, Atmos. Chem. Phys., 7(17), 4639–4659, doi:10.5194/acp-7-4639-2007, 2007.

Ghan, S. J., G., G. and Abdul-Razzak, H.: Competition between Sea Salt and Sulfate Particles as Cloud Condensation Nuclei, J. Atmos. Sci., 55, 3340–3347, 1998.

Gordon, H., Kirkby, J., Baltensperger, U., Bianchi, F., Breitenlechner, M., Curtius, J., Dias, A., Dommen, J., Donahue, N. M., Dunne, E. M., Duplissy, J., Ehrhart, S., Flagan, R. C., Frege, C., Fuchs, C., Hansel, A., Hoyle, C. R., Kulmala, M., Kürten, A., Lehtipalo, K., Makhmutov, V., Molteni, U., Rissanen, M. P., Stozkhov, Y., Tröstl, J., Tsagkogeorgas, G., Wagner, R., Williamson, C., Wimmer, D., Winkler, P. M., Yan, C. and Carslaw, K. S.: Causes and importance of new particle formation in the present-day and preindustrial atmospheres, J. Geophys. Res. Atmos., 122(16), 8739–8760, doi:10.1002/2017JD026844, 2017.

Haywood, J. and Boucher, O.: Estimates of the direct and indirect radiative forcing due to tropospheric aerosols: A review, Rev. Geophys., 38(4), 513–543, doi:10.1029/1999RG000078, 2000.

Herrmann, E., Weingartner, E., Henne, S., L., V., Bukowiecki, N., Steinbacher, M., Conen, F., Collaud Coen, M., Hammer, E., Jurányi, Z., Baltensperger, U., and Gysel, M.: Analysis of long-term aerosol size distribution data from Jungfraujoch with emphasis on free tropospheric conditions, cloud influence, and air mass transport. J. Geophys. Res., 120, 9459–9480, doi:10.1002/2015JD023660, 2015.

Huneeus, N., Schulz, M., Balkanski, Y., Griesfeller, J., Prospero, J., Kinne, S., Bauer, S., Boucher, O., Chin, M., Dentener, F., Diehl, T., Easter, R., Fillmore, D., Ghan, S., Ginoux, P., Grini, A., Horowitz, L., Koch, D., Krol, M. C., Landing, W., Liu, X., Mahowald, N., Miller, R., Morcrette, J. J., Myhre, G., Penner, J., Perlwitz, J., Stier, P., Takemura, T. and Zender, C. S.: Global dust model intercomparison in AeroCom phase i, Atmos. Chem. Phys., 11(15), 7781–7816, doi:10.5194/acp-11-7781-2011, 2011.

Jimenez, J. L., Canagaratna, M. R., Donahue, N. M., Prevot, A. S. H., Zhang, Q., Kroll, J. H., DeCarlo, P. F., Allan, J. D., Coe, H., Ng, N. L., Aiken, A. C., Docherty, K. S., Ulbrich, I. M., Grieshop, A. P., Robinson, A. L., Duplissy, J., Smith, J. D., Wilson, K. R., Lanz, V. A., Hueglin, C., Sun, Y. L., Tian, J., Laaksonen, A., Raatikainen, T., Rautiainen, J., Vaattovaara, P., Ehn, M., Kulmala, M., Tomlinson, J. M., Collins, D. R., Cubison, M. J., Dunlea, E. J., Huffman, J. A., Onasch, T. B., Alfarra, M. R., Williams, P. I., Bower, K., Kondo, Y., Schneider, J., Drewnick, F., Borrmann, S., Weimer, S., Demerjian, K., Salcedo, D., Cottrell, L., Griffin, R., Takami, A., Miyoshi, T., Hatakeyama, S., Shimono, A., Sun, J. Y., Zhang, Y. M., Dzepina, K., Kimmel, J. R., Sueper, D., Jayne, J. T., Herndon, S. C., Trimborn, A. M., Williams, L. R., Wood, E. C., Middlebrook, A. M., Kolb, C. E., Baltensperger, U. and Worsnop, D. R.: Evolution of organic aerosols in the atmosphere, Science (80-.)., 326(5959), 1525–1529, doi:10.1126/science.1180353, 2009.

Johnson, J. S., Regayre, L. A., Yoshioka, M., Pringle, K. J., Lee, L. A., Sexton, D. M. H., Rostron, J. W., Booth, B. B. B. and Carslaw, K. S.: The importance of comprehensive parameter sampling and multiple observations for robust constraint of aerosol radiative forcing, Atmos. Chem. Phys., 18(17), 13031–13053, doi:10.5194/acp-18-13031-2018, 2018.

Jurányi, Z., Gysel, M., Weingartner, E., Bukowiecki, N., Kammermann, L., and Baltensperger, U.: A 17 month climatology of the cloud condensation nuclei number concentration at the high alpine site Jungfraujoch. J. Geophys. Res., 116, D10204, doi:10.1029/2010JD015199, 2011.

Kalivitis, N., Kerminen, V. M., Kouvarakis, G., Stavroulas, I., Bougiatioti, A., Nenes, A., Manninen, H. E., Petäjä, T., Kulmala, M. and Mihalopoulos, N.: Atmospheric new particle formation as a source of CCN in the eastern Mediterranean marine boundary layer, Atmos. Chem. Phys., 15(16), 9203–9215, doi:10.5194/acp-15-9203-2015, 2015.

Kanakidou, M., Seinfeld, J. H., Pandis, S. N., Barnes, I., Dentener, F. J., Facchini, M. C., Van Dingenen, R., Ervens, B., Nenes, A., Nielsen, C. J., Swietlicki, E., Putaud, J. P., Balkanski, Y., Fuzzi, S., Horth, J., Moortgat, G. K., Winterhalter, R., Myhre, C. E. L., Tsigaridis, K., Vignati, E., Stephanou, E. G. and Wilson, J.: Organic aerosol and global climate modelling: a review, Atmos. Chem. Phys., 5(4), 1053–1123, doi:10.5194/acp-5-1053-2005, 2005.

Kanji, Z. A., Ladino, L. A., Wex, H., Boose, Y., Burkert-Kohn, M., Cziczo, D. J. and Krämer, M.: Overview of Ice Nucleating Particles, Meteorol. Monogr., 58, 1.1-1.33, doi:10.1175/AMSMONOGRAPHS-D-16-0006.1, 2017.

Karydis, V. A., Capps, S. L., Russell, A. G. and Nenes, A.: Adjoint sensitivity of global cloud droplet number to aerosol and dynamical parameters, Atmos. Chem. Phys., 12(19), 9041–9055, doi:10.5194/acp-12-9041-2012, 2012.

Kerminen, V. M., Petäjä, T., Manninen, H. E., Paasonen, P., Nieminen, T., Sipilä, M., Junninen, H., Ehn, M., Gagné, S.,

Laakso, L., Riipinen, I., Vehkaṁaki, H., Kurten, T., Ortega, I. K., Dal Maso, M., Brus, D., Hyv̈arinen, A., Lihavainen, H., Leppä, J., Lehtinen, K. E. J., Mirme, A., Mirme, S., Hõrrak, U., Berndt, T., Stratmann, F., Birmili, W., Wiedensohler, A., Metzger, A., Dommen, J., Baltensperger, U., Kiendler-Scharr, A., Mentel, T. F., Wildt, J., Winkler, P. M., Wagner, P. E., Petzold, A., Minikin, A., Plass-Dülmer, C., Pöschl, U., Laaksonen, A. and Kulmala, M.: Atmospheric nucleation: Highlights of the EUCAARI project and future directions, Atmos. Chem. Phys., 10(22), 10829–10848, doi:10.5194/acp-10-10829-2010, 2010.

Kerminen, V. M., Paramonov, M., Anttila, T., Riipinen, I., Fountoukis, C., Korhonen, H., Asmi, E., Laakso, L., Lihavainen, H., Swietlicki, E., Svenningsson, B., Asmi, A., Pandis, S. N., Kulmala, M. and Petäjä, T.: Cloud condensation nuclei production associated with atmospheric nucleation: A synthesis based on existing literature and new results, Atmos. Chem. Phys., 12(24), 12037–12059, doi:10.5194/acp-12-12037-2012, 2012.

Kirkevåg, A., Grini, A., Olivié, D., Seland, Ø., Alterskjær, K., Hummel, M., Karset, I. H. H., Lewinschal, A., Liu, X., Makkonen, R., Bethke, I., Griesfeller, J., Schulz, M. and Iversen, T.: A production-tagged aerosol module for earth system models, OsloAero5.3-extensions and updates for CAM5.3-Oslo, Geosci. Model Dev., 11(10), 3945–3982, doi:10.5194/gmd-11-3945-2018, 2018.

Köhler, H.: The nucleus in and the growth of hygroscopic droplets, Trans. Faraday Soc., 32(0), 1152–1161, doi:10.1039/TF9363201152, 1936.

Kulmala, M. and Kerminen, V. M.: On the formation and growth of atmospheric nanoparticles, Atmos. Res., 90(2–4), 132–150, doi:10.1016/j.atmosres.2008.01.005, 2008.

Kulmala, M., Laaksonen, A. and Pirjola, L.: Parameterizations for sulfuric acid/water nucleation rates, J. Geophys. Res., 103(D7), 8301, doi:10.1029/97JD03718, 1998.

Laaksonen, A., Kulmala, M., O'Dowd, C. D., Joutsensaari, J., Vaattovaara, P., Mikkonen, S., Lehtinen, K. E. J., Sogacheva, L., Dal Maso, M., Aalto, P., Petäjä, T., Sogachev, A., Yoon, Y. J., Lihavainen, H., Nilsson, D., Facchini, M. C., Cavalli, F., Fuzzi, S., Hoffmann, T., Arnold, F., Hanke, M., Sellegri, K., Umann, B., Junkermann, W., Coe, H., Allan, J. D., Alfarra, M. R., Worsnop, D. R., Riekkola, M.-L., Hyötyläinen, T. and Viisanen, Y.: The role of VOC oxidation products in continental new particle formation, Atmos. Chem. Phys., 8(10), 2657–2665, doi:10.5194/acp-8-2657-2008, 2008.

Lee, L. A., Pringle, K. J., Reddington, C. L., Mann, G. W., Stier, P., Spracklen, D. V., Pierce, J. R. and Carslaw, K. S.: The magnitude and causes of uncertainty in global model simulations of cloud condensation nuclei, Atmos. Chem. Phys., 13(17), 8879–8914, doi:10.5194/acp-13-8879-2013, 2013.

Liu, X., Easter, R. ~C. C., Ghan, S. ~J. J., Zaveri, R., Rasch, P., Shi, X., Lamarque, J.-F. F., Gettelman, A., Morrison, H., Vitt, F., Conley, A., Park, S., Neale, R., Hannay, C., Ekman, A. ~M. ~L. M. L., Hess, P., Mahowald, N., Collins, W., Iacono, M. ~J. J., Bretherton, C. ~S. S., Flanner, M. ~G. G. and Mitchell, D.: Toward a minimal representation of aerosols in climate models: Description and evaluation in the Community Atmosphere Model CAM5, Geosci. Model Dev., 5(3), 709–739, doi:10.5194/gmd-5-709-2012, 2012.

Liu, X., Ma, P.-L. L., Wang, H., Tilmes, S., Singh, B., Easter, R. C., Ghan, S. J. and Rasch, P. J.: Description and evaluation of a new four-mode version of the Modal Aerosol Module (MAM4) within version 5.3 of the Community Atmosphere Model, Geosci. Model Dev., 9(2), 505–522, doi:10.5194/gmd-9-505-2016, 2016.

Makkonen, R., Asmi, A., Korhonen, H., Kokkola, H., Järvenoja, S., Räisänen, P., Lehtinen, K. E. J., Laaksonen, A., Kerminen, V.-M., Järvinen, H., Lohmann, U., Bennartz, R., Feichter, J. and Kulmala, M.: Sensitivity of aerosol concentrations and cloud properties to nucleation and secondary organic distribution in ECHAM5-HAM global circulation model, Atmos. Chem. Phys., 9(5), 1747–1766, doi:10.5194/acp-9-1747-2009, 2009.

Mann, G. W., Carslaw, K. S., Ridley, D. A., Spracklen, D. V., Pringle, K. J., Merikanto, J., Korhonen, H., Schwarz, J. P., Lee, L. A., Manktelow, P. T., Woodhouse, M. T., Schmidt, A., Breider, T. J., Emmerson, K. M., Reddington, C. L., Chipperfield, M. P. and Pickering, S. J.: Intercomparison of modal and sectional aerosol microphysics representations within the same 3-D global chemical transport model, Atmos. Chem. Phys., 12(10), 4449–4476, doi:10.5194/acp-12-4449-2012, 2012.

Matsui, H.: Development of a global aerosol model using a two-dimensional sectional method : 1 . Model design, , 1921–1947, doi:10.1002/2017MS000937, 2017.

Metzger, S., Dentener, F., Pandis, S. and Lelieveld, J.: Gas/aerosol partitioning: 1. A computationally efficient model, J. Geophys. Res. Atmos., 107(16), 16-1–24, doi:10.1029/2001JD001102, 2002a.

Metzger, S., Dentener, F., Krol, M., Jeuken, A. and Lelieveld, J.: Gas/aerosol partitioning 2. Global modeling results, J.

Geophys. Res. Atmos., 107(16), 1–23, doi:10.1029/2001JD001103, 2002b.

Moore, R. H., Karydis, V. A., Capps, S. L., Lathem, T. L. and Nenes, A.: Droplet number uncertainties associated with CCN: An assessment using observations and a global model adjoint, Atmos. Chem. Phys., 13(8), 4235–4251, doi:10.5194/acp-13-4235-2013, 2013.

5   Morales Betancourt, R. and Nenes, A.: Understanding the contributions of aerosol properties and parameterization discrepancies to droplet number variability in a global climate model, Atmos. Chem. Phys., 14(9), 4809–4826, doi:10.5194/acp-14-4809-2014, 2014.

Morales, R. and Nenes, A.: Characteristic updrafts for computing distribution-averaged cloud droplet number and stratocumulus cloud properties, J. Geophys. Res. Atmos., 115(18), 2–9, doi:10.1029/2009JD013233, 2010.

10   Nenes, A. and Seinfeld, J. H.: Parameterization of cloud droplet formation in global climate models, J. Geophys. Res. Atmos., 108(D14), 4415, doi:10.1029/2002JD002911, 2003.

Ovadnevaite, J., Ceburnis, D., Leinert, S., Dall'Osto, M., Canagaratna, M., O'Doherty, S., Berresheim, H. and O'Dowd, C.: Submicron NE Atlantic marine aerosol chemical composition and abundance: Seasonal trends and air mass categorization, J. Geophys. Res. Atmos., 119(20), 11,850-11,863, doi:10.1002/2013JD021330, 2014.

15   Petters, M. D. and Kreidenweis, S. M.: A single parameter representation of hygroscopic growth and cloud\ncondensation nucleus activity, Atmos. Chem. Phys., 1961–1971, doi:10.5194/acp-7-1961-2007, 2007.

Petters, M. D., Kreidenweis, S. M., Sandu, A., Verwer, J. G., van Loon, M., Carmichael, G. R., Potra, F. A., Dabdub, D. and Seinfeld, J. H.: A single parameter representation of hygroscopic growth and cloud condensation nucleus activity, Atmos. Chem. Phys., 7(8), 1961–1971, doi:10.5194/acp-7-1961-2007, 2007.

20   Pierce, J. R., Riipinen, I., Kulmala, M., Ehn, M., Petäjä, T., Junninen, H., Worsnop, D. R. and Donahue, N. M.: Quantification of the volatility of secondary organic compounds in ultrafine particles during nucleation events, Atmos. Chem. Phys., 11(17), 9019–9036, doi:10.5194/acp-11-9019-2011, 2011.

Pringle, K. J., Tost, H., Pozzer, A., Pöschl, U. and Lelieveld, J.: Global distribution of the effective aerosol hygroscopicity parameter for CCN activation, Atmos. Chem. Phys., 10(12), 5241–5255, doi:10.5194/acp-10-5241-2010, 2010.

25   Pruppacher, H. R. and Klett, J. D.: Microphysics of clouds and precipitation, 2nd ed., Kluwer Academic Publishers, Dordrecht, The Netherlands., 1997.

Reutter, P., Su, H., Trentmann, J., Simmel, M., Rose, D., Gunthe, S. S., Wernli, H., Andreae, M. O. and Pöschl, U.: Aerosol- and updraft-limited regimes of cloud droplet formation: influence of particle number, size and hygroscopicity on the activation of cloud condensation nuclei (CCN), Atmos. Chem. Phys., 9, 7067–7080 [online] Available from:
30   https://www.atmos-chem-phys.net/9/7067/2009/, 2009.

Riccobono, F., Schobesberger, S., Scott, C. E., Dommen, J., Ortega, I. K., Rondo, L., Almeida, J., Amorim, A., Bianchi, F., Breitenlechner, M., David, A., Downard, A., Dunne, E. M., Duplissy, J., Ehrhart, S., Flagan, R. C., Franchin, A., Hansel, A., Junninen, H., Kajos, M., Keskinen, H., Kupc, A., Kürten, A., Kvashin, A. N., Laaksonen, A., Lehtipalo, K., Makhmutov, V., Mathot, S., Nieminen, T., Onnela, A., Petäjä, T., Praplan, A. P., Santos, F. D., Schallhart, S., Seinfeld, J.
35   H., Sipilä, M., Spracklen, D. V, Stozhkov, Y., Stratmann, F., Tomé, A., Tsagkogeorgas, G., Vaattovaara, P., Viisanen, Y., Vrtala, A., Wagner, P. E., Weingartner, E., Wex, H., Wimmer, D., Carslaw, K. S., Curtius, J., Donahue, N. M., Kirkby, J., Kulmala, M., Worsnop, D. R. and Baltensperger, U.: Oxidation Products of Biogenic Emissions Contribute to Nucleation of Atmospheric Particles, Science (80-.)., 344(6185), 717–721, 2014.

Schmale, J., Henning, S., Henzing, B., Keskinen, H., Sellegri, K., Ovadnevaite, J., Bougiatioti, A., Kalivitis, N., Stavroulas,
40   I., Jefferson, A., Park, M., Schlag, P., Kristensson, A., Iwamoto, Y., Pringle, K., Reddington, C., Aalto, P., Äijälä, M., Baltensperger, U., Bialek, J., Birmili, W., Bukowiecki, N., Ehn, M., Fjæraa, A. M., Fiebig, M., Frank, G., Fröhlich, R., Frumau, A., Furuya, M., Hammer, E., Heikkinen, L., Herrmann, E., Holzinger, R., Hyono, H., Kanakidou, M., Kiendler-Scharr, A., Kinouchi, K., Kos, G., Kulmala, M., Mihalopoulos, N., Motos, G., Nenes, A., O'Dowd, C., Paramonov, M., Petäjä, T., Picard, D., Poulain, L., Prévôt, A. S. H., Slowik, J., Sonntag, A., Swietlicki, E., Svenningsson, B., Tsurumaru,
45   H., Wiedensohler, A., Wittbom, C., Ogren, J. A., Matsuki, A., Yum, S. S., Myhre, C. L., Carslaw, K., Stratmann, F. and Gysel, M.: Collocated observations of cloud condensation nuclei, particle size distributions, and chemical composition, Sci. Data, 4, 170003, doi:10.1038/sdata.2017.3, 2017a.

Schmale, J., Henning, S., Decesari, S., Henzing, B., Keskinen, H., Paramonov, M., Sellegri, K., Ovadnevaite, J., Pöhlker, M. L., Brito, J., Bougiatioti, A., Kristensson, A., Kalivitis, N., Stavroulas, I., Carbone, S., Jefferson, A., Park, M., Schlag, P.,
50   Iwamoto, Y., Aalto, P., Äijälä, M., Bukowiecki, N., Ehn, M., Frank, G., Fröhlich, R., Frumau, A., Herrmann, E.,

Herrmann, H., Holzinger, R., Kos, G., Kulmala, M., Mihalopoulos, N., Nenes, A., O'Dowd, C., Petäjä, T., Picard, D., Pöhlker, C., Pöschl, U., Poulain, L., Prévôt, A. S. H., Swietlicki, E., Andreae, M. O., Artaxo, P., Wiedensohler, A., Ogren, J., Matsuki, A., Yum, S. S., Stratmann, F., Baltensperger, U. and Gysel, M.: What do we learn from long-term cloud condensation nuclei number concentration, particle number size distribution, and chemical composition measurements at regionally representative observatories?, Atmos. Chem. Phys. Discuss., (August), 1–51, doi:10.5194/acp-2017-798, 2017b.

Schutgens, N. A. J., Gryspeerdt, E., Weigum, N., Tsyro, S., Goto, D., Schulz, M. and Stier, P.: Will a perfect model agree with perfect observations ? The impact of spatial sampling, , 6335–6353, doi:10.5194/acp-16-6335-2016, 2016.

Seinfeld, J. H., Bretherton, C., Carslaw, K. S., Coe, H., DeMott, P. J., Dunlea, E. J., Feingold, G., Ghan, S., Guenther, A. B., Kahn, R., Kraucunas, I., Kreidenweis, S. M., Molina, M. J., Nenes, A., Penner, J. E., Prather, K. A., Ramanathan, V., Ramaswamy, V., Rasch, P. J., Ravishankara, A. R., Rosenfeld, D., Stephens, G. and Wood, R.: Improving our fundamental understanding of the role of aerosol−cloud interactions in the climate system, Proc. Natl. Acad. Sci., 113(21), 5781–5790, doi:10.1073/pnas.1514043113, 2016.

Sotiropoulou, R.-E. P., Medina, J. and Nenes, A.: CCN predictions: Is theory sufficient for assessments of the indirect effect?, Geophys. Res. Lett., 33(5), L05816, doi:10.1029/2005GL025148, 2006.

Sotiropoulou, R. E. P., Nenes, A., Adams, P. J. and Seinfeld, J. H.: Cloud condensation nuclei prediction error from application of Köhler theory: Importance for the aerosol indirect effect, J. Geophys. Res. Atmos., 112(12), D12202, doi:10.1029/2006JD007834, 2007.

Spracklen, D. V., Carslaw, K. S., Merikanto, J., Mann, G. W., Reddington, C. L., Pickering, S., Ogren, J. A., Andrews, E., Baltensperger, U., Weingartner, E., Boy, M., Kulmala, M., Laakso, L., Lihavainen, H., Kivekäs, N., Komppula, M., Mihalopoulos, N., Kouvarakis, G., Jennings, S. G., O'Dowd, C., Birmili, W., Wiedensohler, A., Weller, R., Gras, J., Laj, P., Sellegri, K., Bonn, B., Krejci, R., Laaksonen, A., Hamed, A., Minikin, A., Harrison, R. M., Talbot, R. and Sun, J.: Explaining global surface aerosol number concentrations in terms of primary emissions and particle formation, Atmos. Chem. Phys., 10(10), 4775–4793, doi:10.5194/acp-10-4775-2010, 2010.

Spracklen, D. V., Carslaw, K. S., Pöschl, U., Rap, A. and Forster, P. M.: Global cloud condensation nuclei influenced by carbonaceous combustion aerosol, Atmos. Chem. Phys., 11(17), 9067–9087, doi:10.5194/acp-11-9067-2011, 2011.

Spracklen, D. V, Bonn, B. and Carslaw, K. S.: Boreal forests, aerosols and the impacts on clouds and climate., Philos. Trans. A. Math. Phys. Eng. Sci., 366(1885), 4613–26, doi:10.1098/rsta.2008.0201, 2008.

Sullivan, R. C., Moore, M. J. K., Petters, M. D., Kreidenweis, S. M., Roberts, G. C. and Prather, K. A.: Effect of chemical mixing state on the hygroscopicity and cloud nucleation properties of calcium mineral dust particles, Atmos. Chem. Phys., 9(10), 3303–3316, doi:10.5194/acp-9-3303-2009, 2009.

Sullivan, S. C., Lee, D., Oreopoulos, L. and Nenes, A.: Role of updraft velocity in temporal variability of global cloud hydrometeor number, Proc. Natl. Acad. Sci., 113(21), 5791–5796, doi:10.1073/pnas.1514039113, 2016.

Textor, C., Schulz, M., Guibert, S., Kinne, S., Balkanski, Y., Bauer, S., Berntsen, T., Berglen, T., Boucher, O., Chin, M., Dentener, F., Diehl, T., Easter, R., Feichter, H., Fillmore, D., Ghan, S., Ginoux, P., Gong, S., Grini, a., Hendricks, J., Horowitz, L., Huang, P., Isaksen, I., Iversen, T., Kloster, S., Koch, D., Kirkevåg, a., Kristjansson, J. E., Krol, M., Lauer, a., Lamarque, J. F., Liu, X., Montanaro, V., Myhre, G., Penner, J., Pitari, G., Lamarque, J. F., Liu, X., Montanaro, V., Myhre, G., Penner, J., Pitari, G., Reddy, S., Seland, Ø., Stier, P., Takemura, T. and Tie, X.: Analysis and quantification of the diversities of aerosol life cycles within AeroCom, Atmos. Chem. Phys., 6, 1777–1813, doi:10.5194/acpd-5-8331-2005, 2006.

Tröstl, J., Chuang, W. K., Gordon, H., Heinritzi, M., Yan, C., Molteni, U., Ahlm, L., Frege, C., Bianchi, F., Wagner, R., Simon, M., Lehtipalo, K., Williamson, C., Craven, J. S., Duplissy, J., Adamov, A., Almeida, J., Bernhammer, A. K., Breitenlechner, M., Brilke, S., Dias, A., Ehrhart, S., Flagan, R. C., Franchin, A., Fuchs, C., Guida, R., Gysel, M., Hansel, A., Hoyle, C. R., Jokinen, T., Junninen, H., Kangasluoma, J., Keskinen, H., Kim, J., Krapf, M., Kürten, A., Laaksonen, A., Lawler, M., Leiminger, M., Mathot, S., Möhler, O., Nieminen, T., Onnela, A., Petäjä, T., Piel, F. M., Miettinen, P., Rissanen, M. P., Rondo, L., Sarnela, N., Schobesberger, S., Sengupta, K., Sipilä, M., Smith, J. N., Steiner, G., Tomè, A., Virtanen, A., Wagner, A. C., Weingartner, E., Wimmer, D., Winkler, P. M., Ye, P., Carslaw, K. S., Curtius, J., Dommen, J., Kirkby, J., Kulmala, M., Riipinen, I., Worsnop, D. R., Donahue, N. M. and Baltensperger, U.: The role of low-volatility organic compounds in initial particle growth in the atmosphere, Nature, 533(7604), 527–531, doi:10.1038/nature18271, 2016.

Tsigaridis, K., Koch, D. and Menon, S.: Uncertainties and importance of sea spray composition on aerosol direct and indirect effects, J. Geophys. Res. Atmos., 118(1), 220–235, doi:10.1029/2012JD018165, 2013.

Tsigaridis, K., Daskalakis, N., Kanakidou, M., Adams, P. J., Artaxo, P., Bahadur, R., Balkanski, Y., Bauer, S. E., Bellouin, N., Benedetti, A., Bergman, T., Berntsen, T. K., Beukes, J. P., Bian, H., Carslaw, K. S., Chin, M., Curci, G., Diehl, T., Easter, R. C., Ghan, S. J., Gong, S. L., Hodzic, A., Hoyle, C. R., Iversen, T., Jathar, S., Jimenez, J. L., Kaiser, J. W., Kirkevåg, A., Koch, D., Kokkola, H., Lee, Y. H., Lin, G., Liu, X., Luo, G., Ma, X., Mann, G. W., Mihalopoulos, N., Morcrette, J.-J., Müller, J.-F., Myhre, G., Myriokefalitakis, S., Ng, N. L., O'Donnell, D., Penner, J. E., Pozzoli, L., Pringle, K. J., Russell, L. M., Schulz, M., Sciare, J., Seland, Ø., Shindell, D. T., Sillman, S., Skeie, R. B., Spracklen, D., Stavrakou, T., Steenrod, S. D., Takemura, T., Tiitta, P., Tilmes, S., Tost, H., van Noije, T., van Zyl, P. G., von Salzen, K., Yu, F., Wang, Z., Wang, Z., Zaveri, R. A., Zhang, H., Zhang, K., Zhang, Q. and Zhang, X.: The AeroCom evaluation and intercomparison of organic aerosol in global models, Atmos. Chem. Phys., 14(19), 10845–10895, doi:10.5194/acp-14-10845-2014, 2014.

Vehkamäki, H.: An improved parameterization for sulfuric acid–water nucleation rates for tropospheric and stratospheric conditions, J. Geophys. Res., 107(D22), 4622, doi:10.1029/2002JD002184, 2002.

Vignati, E., Wilson, J. and Stier, P.: M7: An efficient size-resolved aerosol microphysics module for large-scale aerosol transport models, J. Geophys. Res. Atmos., 109(D22), n/a-n/a, doi:10.1029/2003JD004485, 2004.

Yu, F.: A secondary organic aerosol formation model considering successive oxidation aging and kinetic condensation of organic compounds: Global scale implications, Atmos. Chem. Phys., 11(3), 1083–1099, doi:10.5194/acp-11-1083-2011, 2011.

Yu, F. and Luo, G.: Simulation of particle size distribution with a global aerosol model: contribution of nucleation to aerosol and CCN number concentrations, Atmos. Chem. Phys. Discuss., 9(2), 10597–10645, doi:10.5194/acpd-9-10597-2009, 2009.

Yu, F., Nadykto, A. B., Herb, J., Luo, G., Nazarenko, K. M. and Uvarova, L. A.: H2SO4–H2O–NH3 ternary ion-mediated nucleation (TIMN): kinetic-based model and comparison with CLOUD measurements, Atmos Chem Phys, 18, 17451–17474, doi:doi.org/10.5194/acp-18-17451-2018, 2018.

Table 1. Hygroscopicity parameters used by the participating models for water uptake calculations.

MODEL	SO4	OA	SS	DU	BC	NO3
CAM5-chem-APM	0.9	0.1	1.28	0	0	0.9
CAM5-chem-ATRAS2	0.61	0.1	1.16	0.001	1.e-6	0.61
CAM5_MAM3	0.507	0.1	1.16	0.068	0	N/A
CAM5_MAM4	0.507	0	1.16	0.068		N/A
CAM5.3-Oslo	0.507	0.14	1.2	0.069	1.e-7	N/A
ECHAM5.5-HAM2-ELVOC_UH	0.6	0.06	1.12	0		
ECHAM6-HAM2 [1]	0.7	0.	1.3	0	0	N/A
ECHAM6-HAM2-AP[1]	0.7	0	1.3[3]	0	0	N/A
EMAC [2]		0.1	1.12	0	0	N/A
GEOS-Chem-APM	0.9	0.1	1.28	0	0	0.9
GEOS-Chem-TOMAS	1.0	0.1[4]	1.2	0.01	0	N/A
GISS-E2.1-MATRIX	0.507	0.141	1.335	0.14	5.e-7	0.507
GISS-E2-TOMAS	0.7	0.15[5]	1.3	0	0	N/A
TM4-ECPL	0.6	0.1	1.0	0	0	N/A
TM5	0.6	0.1	1.0 [6]	0	0	0.6

[1] ECHAM6-HAM2 uses the Abdul-Razzak and Ghan (AR-G) activation scheme (Abdul Razzak and Ghan, 2000). The reported values are approximated using the number of ions and osmotic coefficients used in the AR-G scheme.

[2] EMAC model simulates the effective hygroscopicity parameter κ of each aerosol size mode in order to describe the influence of chemical composition on the CCN activity of aerosol particles (Pringle et al., 2010). These values are the internally mixed κ calculated across the nucleation, Aitken, accumulation and coarse modes. The effective aerosol hygroscopicity parameter κ is calculated according to the simple mixing rule proposed by (Petters et al., 2007) using the volume fraction and hygroscopicity parameter of each chemical component (23 salts from ISORROPIA-II and 4 bulk species) taken from (Petters et al., 2007) and (Sullivan et al., 2009)

[3] Approximate kappa values computed from the water activity used for activation in ECHAM6-HAM2-AP

[4] for hydrophilic OA $\kappa=0.1$, for hydrophobic OA $\kappa=0.01$

[5] for hydrophilic ORG. For hydrophobic, $\kappa=0$.

[6] for NaCl $\kappa=1$, for Na_2SO_4 $\kappa=0.95$
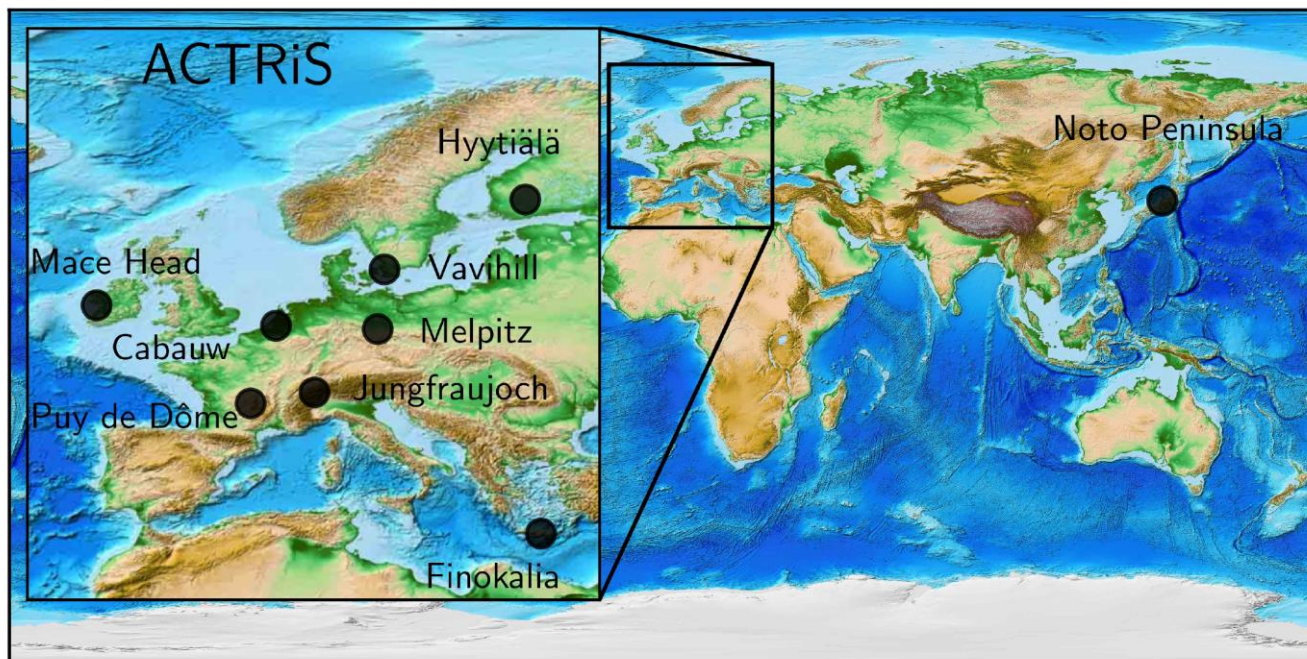
Fig. 1. Map showing the location of the measurements sites used in this study.
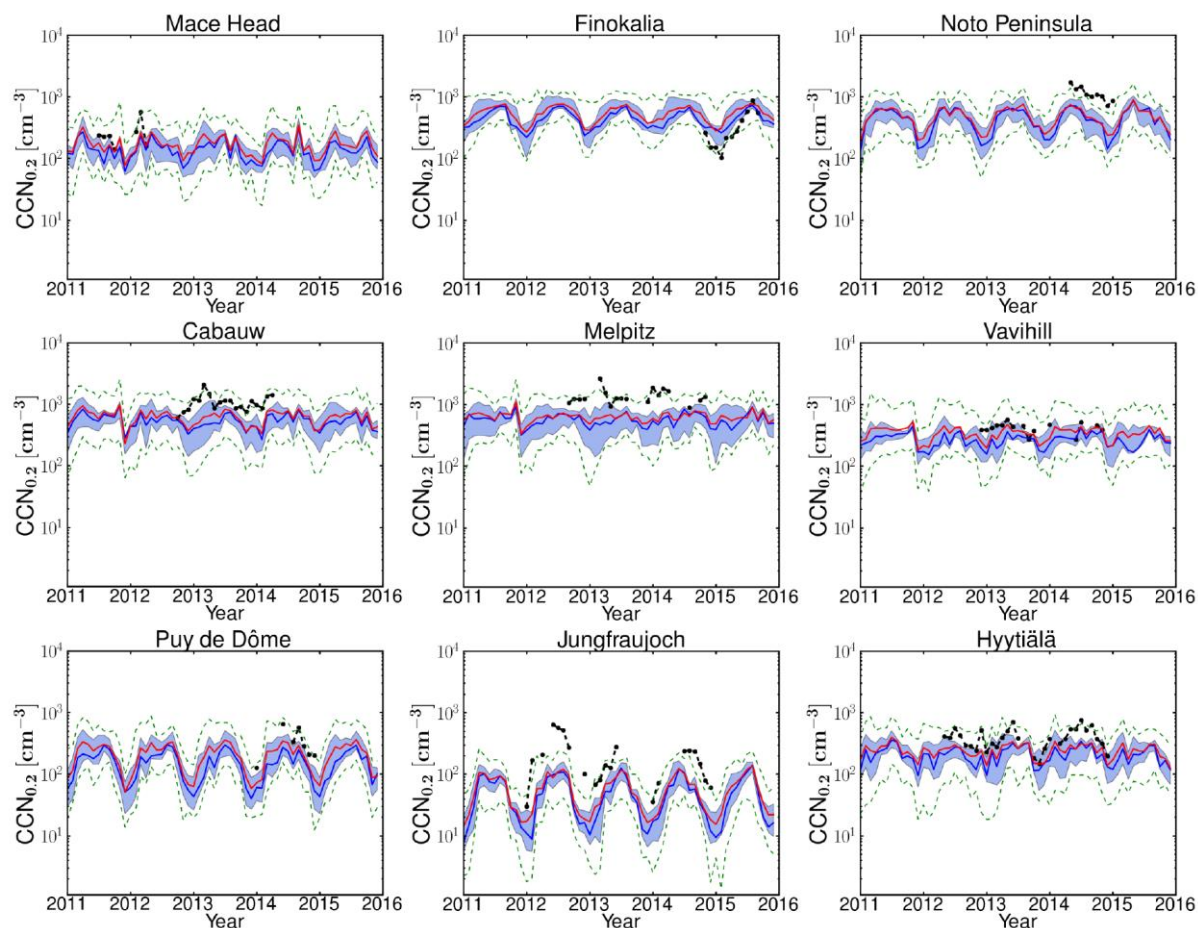
Fig. 2. Monthly ensembles for the years 2011-2015 of the CCN number concentration for supersaturation 0.2 % ($CCN_{0.2}$). The $CCN_{0.2}$ obtained from observational data is shown with dots and dashed lines. The continuous bold blue and red lines show the monthly median and mean of the all models, respectively. The shaded area shows the 25/75% of the model results, while the green dashed lines the minimum and maximum values of all models.
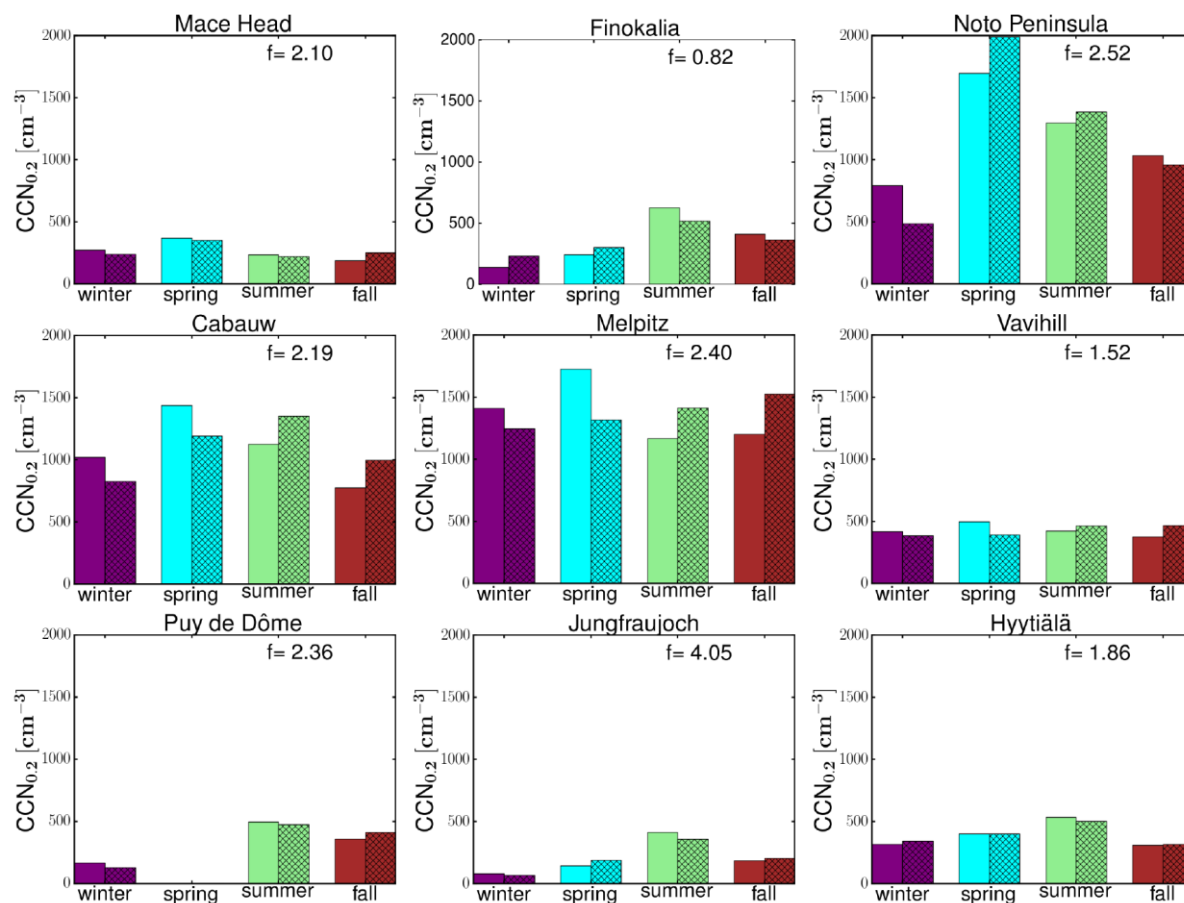
Fig.3. Comparison of the seasonal variations of the observed and model-median computed $CCN_{0.2}$. The solid bars show the average of the observed $CCN_{0.2}$ during each season and the shaded bars the corresponding averages of the model results. The simulated $CCN_{0.2}$ concentrations have been scaled by a factor, f (denoted in each graph), so that the four seasons mean is the same as the observed one. For Puy de Dôme normalization is based on the mean of three seasons (winter, summer and fall) due to data availability.
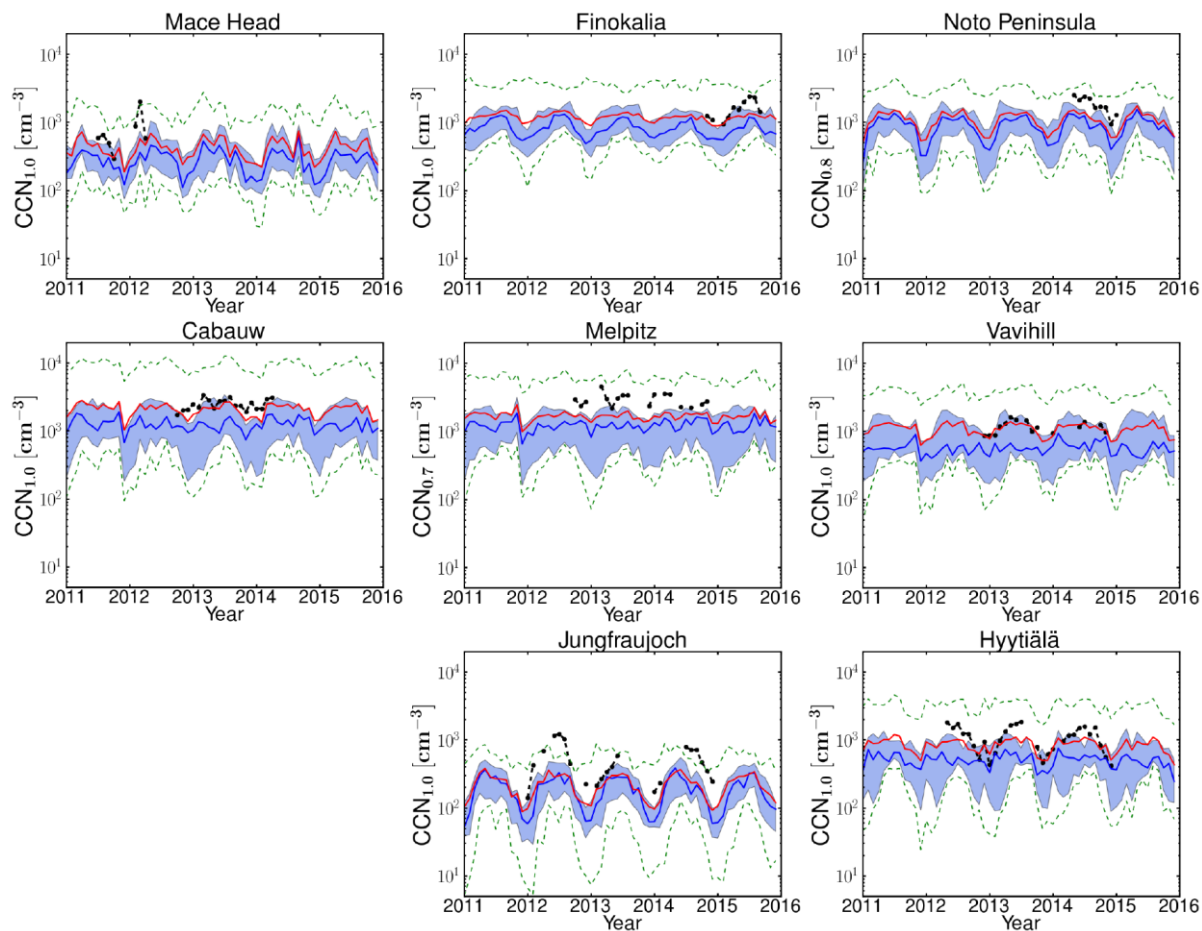
Fig. 4. Same as Figure 2 for the CCN at the maximum supersaturation with available measurements at each station. For Puy de Dôme only $CCN_{0.2}$ data are available and are shown in Figure 2.
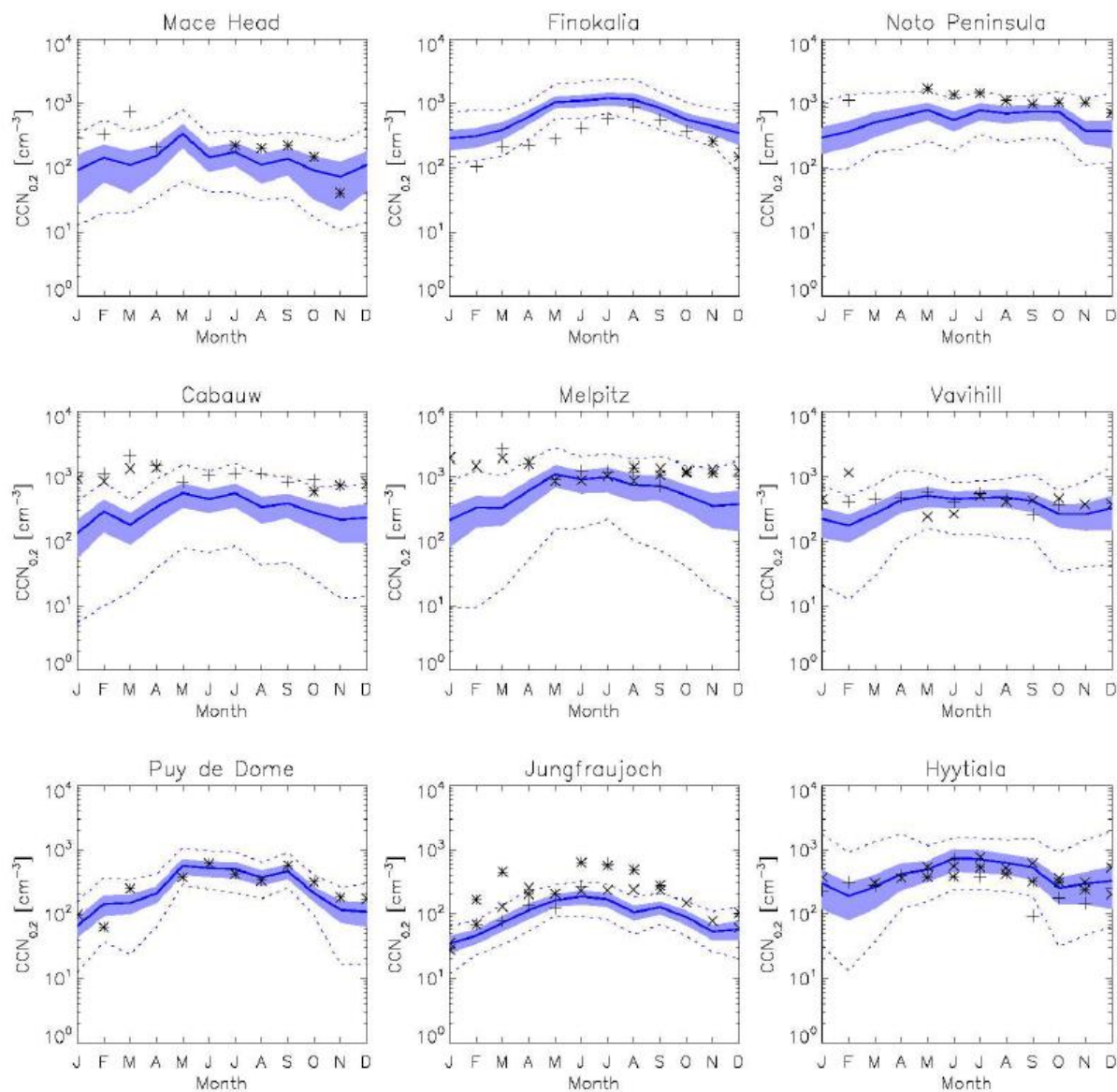
Fig. 5. Monthly average $CCN_{0.2}$ based on HadGEM3-UKCA perturbed parameter ensemble simulations for year 2008. The solid blue line shows the mean of 260,000 model emulators for each month and station. The shaded area shows the range of emulator mean plus and minus one standard deviation, while the blue dashed lines show the minimum and maximum emulator values. The $CCN_{0.2}$ obtained from observational data are shown in symbols; stars, pluses and crosses for three different years with available data.
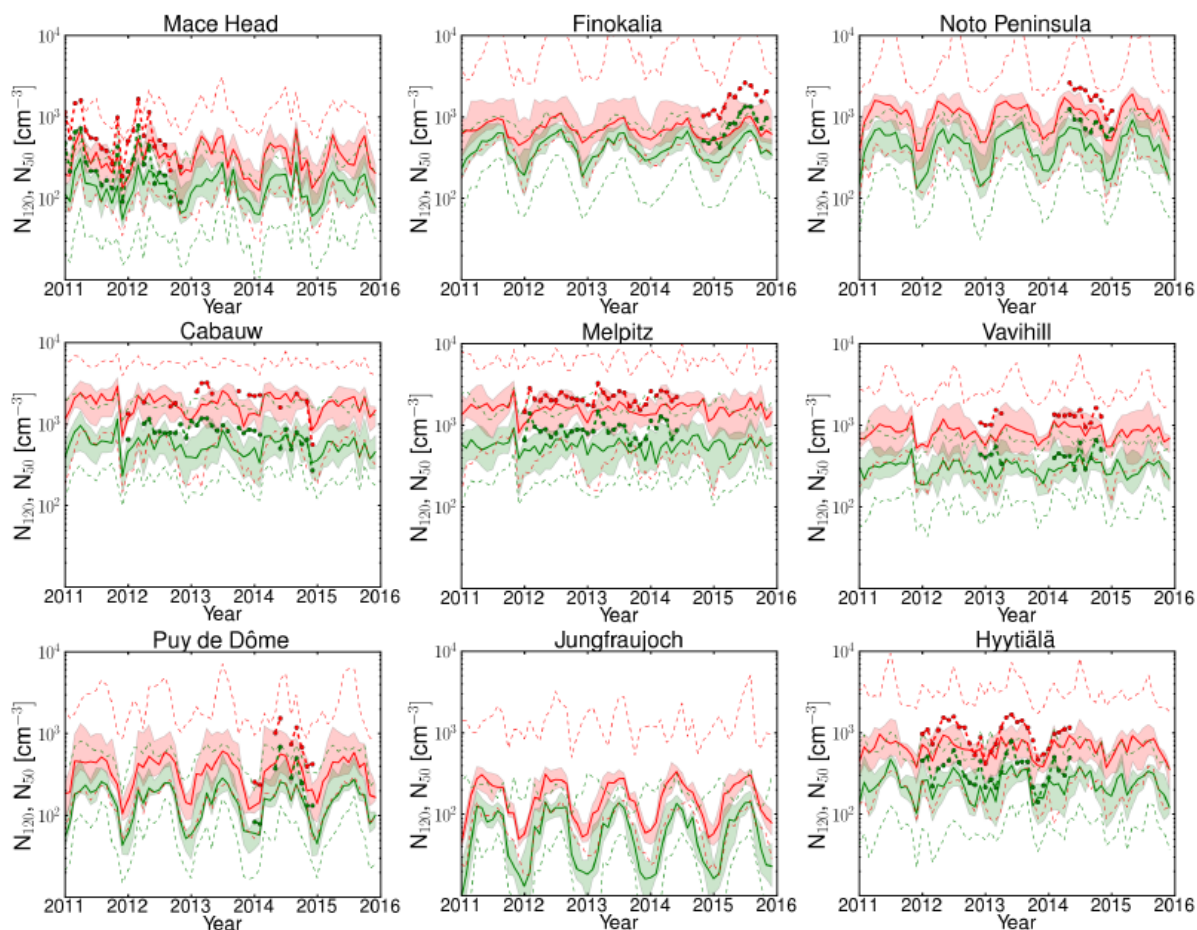
Fig. 6. Monthly ensembles for the period 2011-2015 of the number concentration of particles with diameters larger than 50 nm (N_{50} – in red) and 120 nm (N_{120} – in green). The continuous lines correspond to the median of the models for each month, the shaded areas show the 25/75% quartiles and the dashed lines the minimum and maximum of all models for the N_{50} (red area) and N_{120} (green area). Observational data are available for all stations except Jungfraujoch and are shown with bold points and dashed lines of the corresponding color.
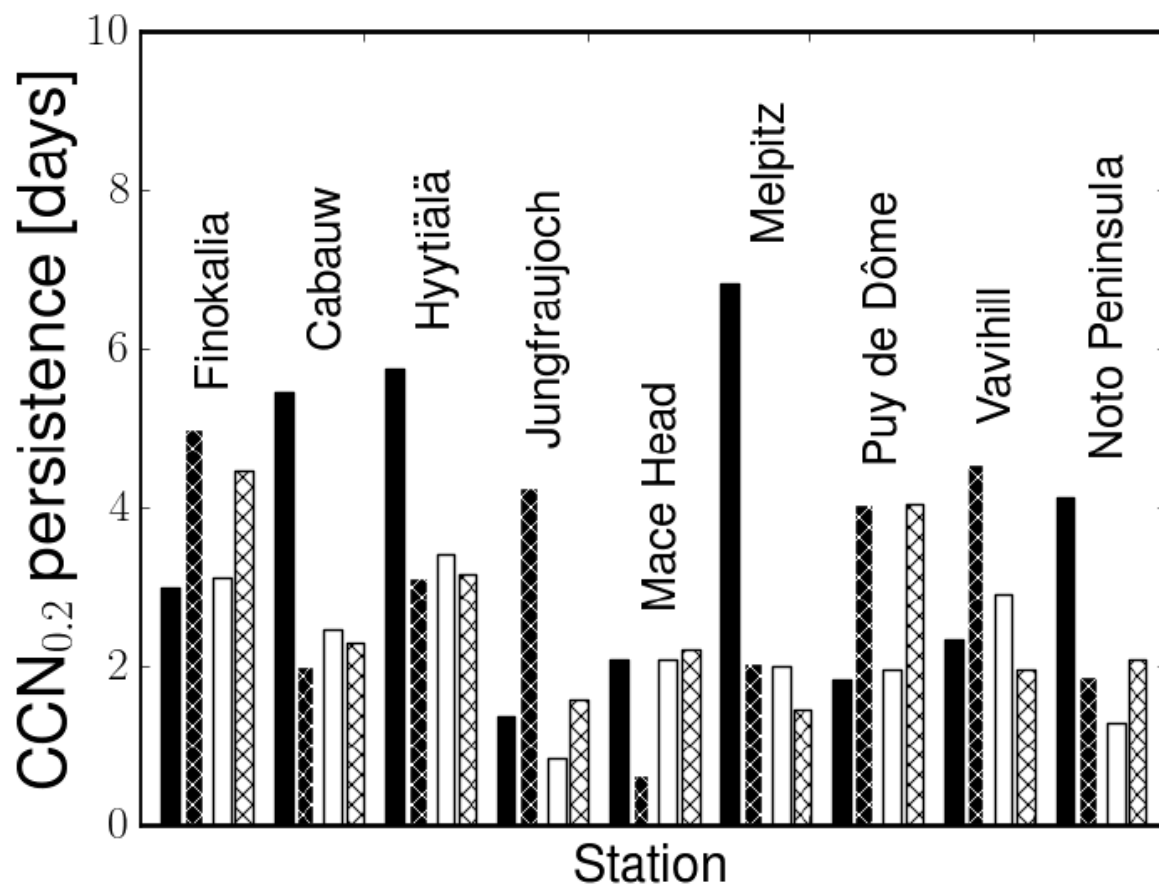
Fig. 7. Comparison between the observed and the mean of the model derived persistence (days) of $CCN_{0.2}$ during winter (left bar) and summer (right shaded bar) for each station. The observed persistence times are shown in black for each station and the mean of the model-derived persistence times in white. The persistence times (in days) obtained from model simulations have been computed at the same time periods as the observed ones.
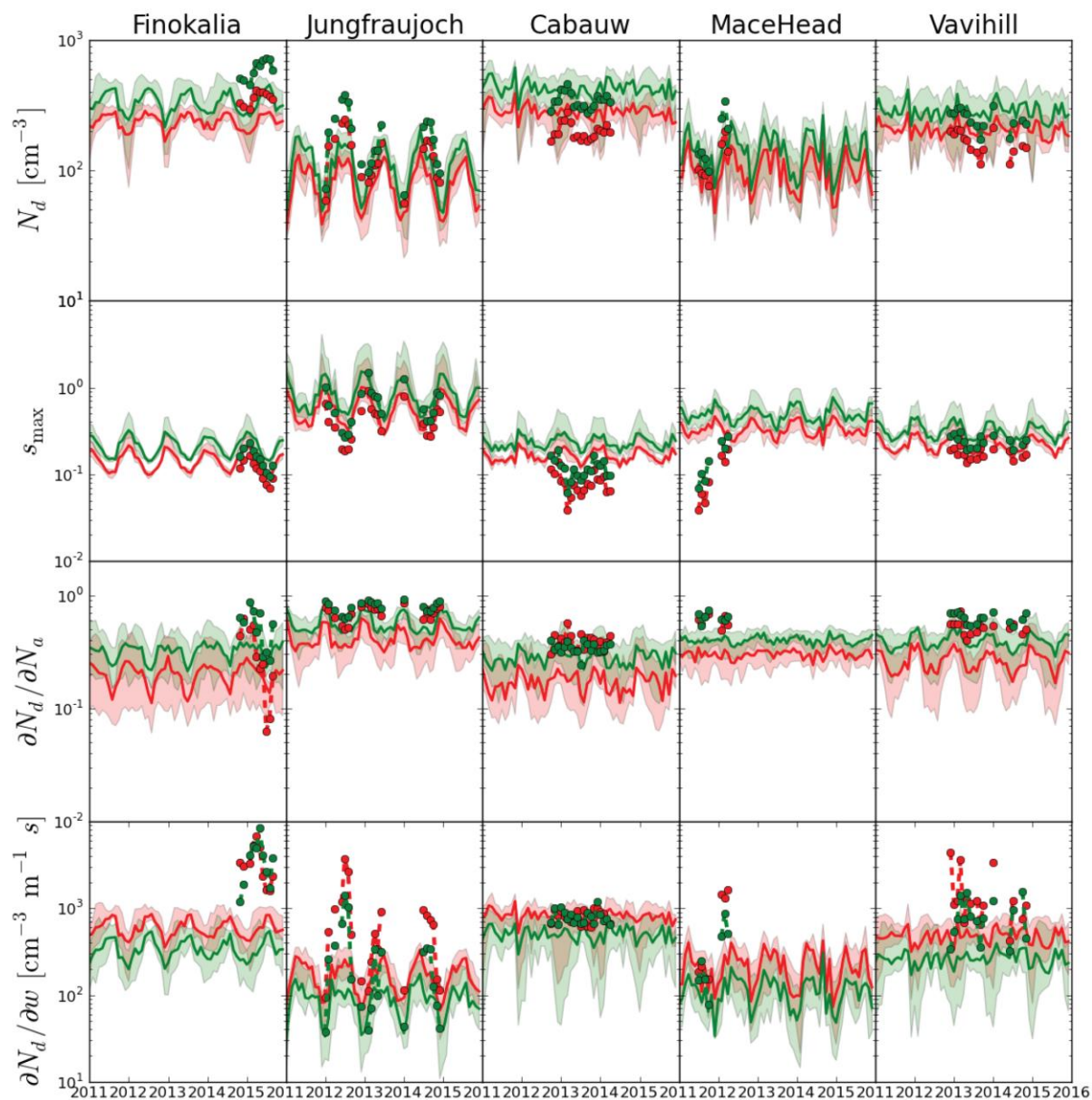
Fig. 8. Comparison between the observed (dashed lines and circles) and the monthly averages of all models (continuous lines) of the cloud droplet properties; in red for updraft velocity w=0.3 ms⁻¹ and in green for updraft velocity w=0.6 ms⁻¹. For each station from top to bottom the four graphs show (as indicated in the y-axis label), the number of cloud droplets, N_d, the maximum supersaturation, s_{max}, the sensitivity of the N_d to the total number of aerosol particles, $(\partial N_d/\partial N_a)$, and the sensitivity of the N_d to the updraft velocity $(\partial N_d/\partial w)$.
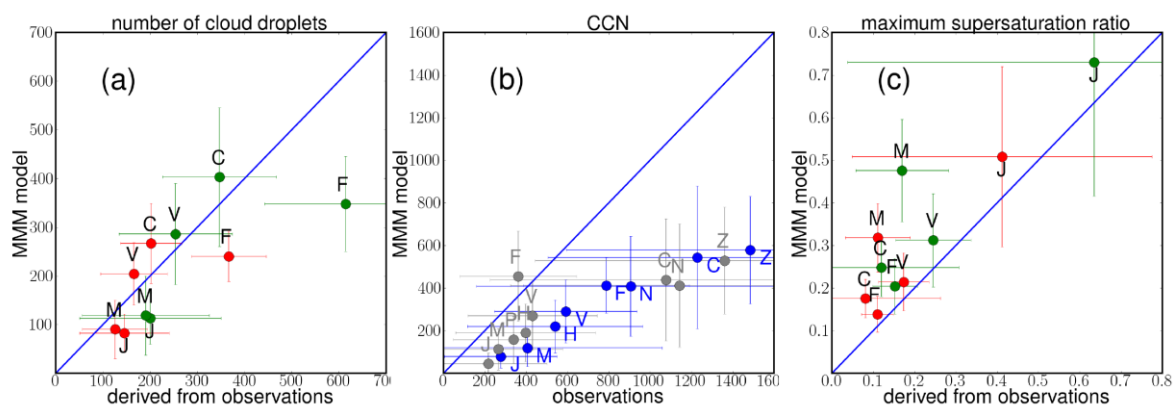
Fig. 9. Scatter plot of the average values of multi-model median results (*y*-axis) versus observationally-derived results (*x*-axis) for : (a) CDNC (N_d) (in cm^{-3}) in red for updraft velocity $w = 0.3\,ms^{-1}$ and in green for updraft velocity $w = 0.6\,ms^{-1}$, (b) CCN at supersaturation 0.2% (gray) and CCN at maximum supersaturation (blue) with available data (in cm^{-3}). To fit the scale all blue colored values have been divided by 2. (c) as (a) but for s_{max} (in %). The letters close to the symbols indicate the station names (C - Cabauw, F - Finokalia, H - Hyytiälä, J - Jungfraujoch, M - Mace Head, N - Noto Peninsula, P - Puy de Dôme, V - Vavihill, and Z - Melpitz)
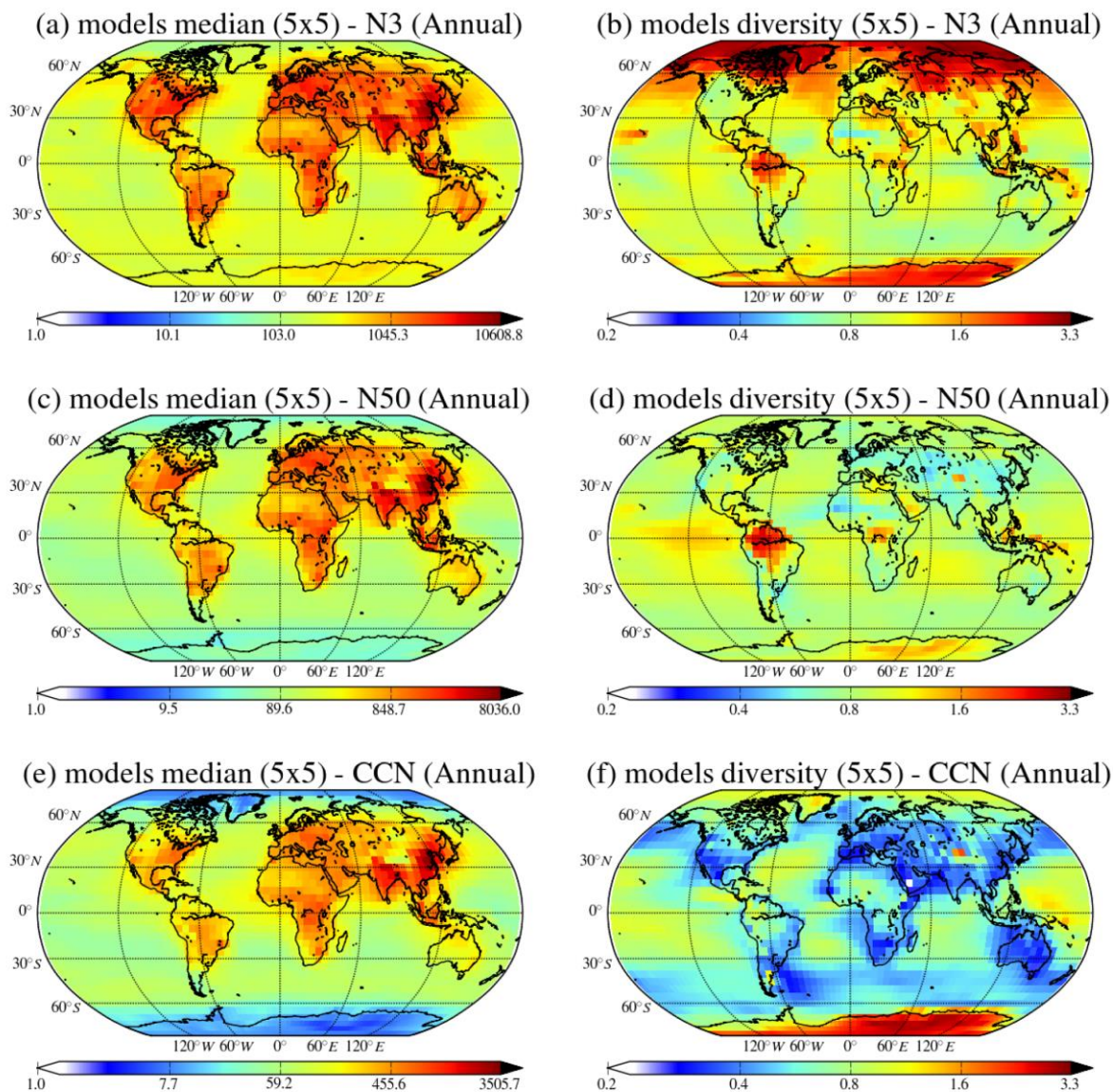
Fig. 10. Global distributions of the annual multi-model median concentrations of the N_3, N_{50} and $CCN_{0.2}$ for the year 2011 (a, c, e respectively) and the corresponding diversities (b, d, f, respectively; calculated as the ratio of standard deviation to the mean of the models).
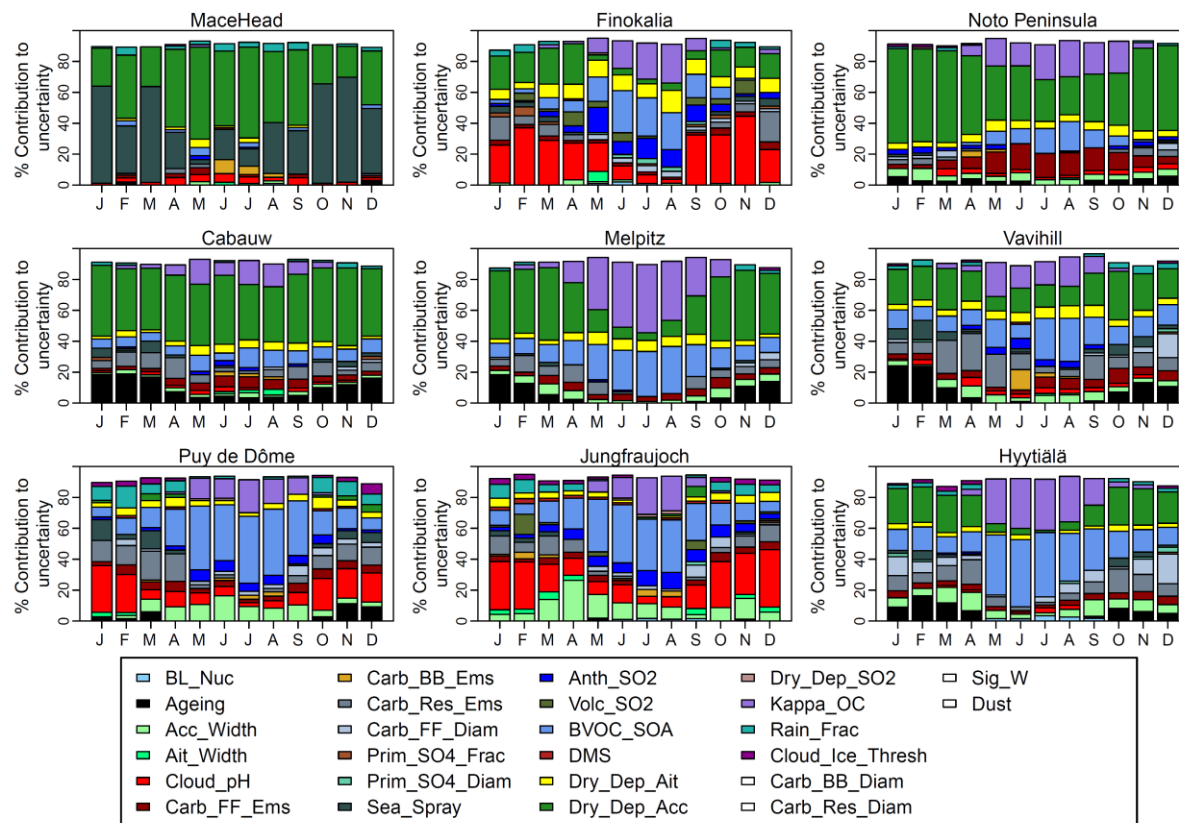
Fig. 11. Contribution to the uncertainty in monthly average $CCN_{0.2}$ based on HadGEM3-UKCA perturbed parameter ensemble simulations for year 2008. Each colour refers to one of the 26 perturbed parameters as indicated in the legend of the figure. The uncertainty is shown as the percentage contribution of the parameter to the $CCN_{0.2}$ variance. The assumed parameter uncertainty ranges are given in Yoshioka et al. (in prep).